

Quantum metasurfaces as probes of vacuum particle content

Germain Tobar,^{1,*} Joshua Foo,² Sofia Qvarfort,^{1,3} Fabio Costa,³ Rivka Bekenstein,⁴ and Magdalena Zych^{1,†}

¹*Department of Physics, Stockholm University, SE-106 91 Stockholm, Sweden*

²*Department of Physics and Astronomy, University of Waterloo, Waterloo, Ontario, Canada, N2L 3G1*

³*Nordita, KTH Royal Institute of Technology and Stockholm University,*

Hannes Alfvens vag 12, SE-114 19 Stockholm, Sweden

⁴*Racah Institute of Physics, The Hebrew University of Jerusalem, Jerusalem 91904, Israel*

(Dated: February 16, 2026)

The quantum vacuum of the electromagnetic field is inherently entangled across distinct spatial sub-regions, resulting in entangled particle content across these sub-regions. However, accessing this particle content in a controlled laboratory experiment has remained out of experimental reach. Here we propose to overcome this challenge with a quantum mirror made from a two-dimensional sub-wavelength array of atoms that divides a photonic cavity. The array's response to light is tunable between transmissive and reflective states by a control atom that is excited to a Rydberg state. We find that vacuum photon content from non-perturbative changes of the boundary conditions and therefore distinct spatial sub-regions of the vacuum causes subtle frequency shifts that are accessible to sub-wavelength atom array platforms. This novel approach for probing vacuum particle content stems from the system's unique ability to create coherent dynamics of superpositions of transmissive and reflective states, providing a quantum-enhanced platform for observing vacuum particle creation from highly non-perturbative boundary condition changes of the electromagnetic field vacuum.

I. INTRODUCTION

In any relativistic quantum field theory, including quantum electrodynamics (QED), local regions of the field are not in the vacuum state even when the global field is in the vacuum [1–5]. This is because vacuum states of field theories contain local fluctuations. The key physical consequence of this phenomenon is the prediction of non-zero particle content in sub-regions of a quantum field that is in its global vacuum state. Various cavity QED experiments have explored the unique properties of the QED vacuum, such as the cooperative Lamb shift observed in atomic ensembles [6, 7]. A significant challenge in modern vacuum QED experiments is detecting particle content from the vacuum, where photons from spatial sub-regions of the vacuum become observable. This phenomenon occurs in a QED system when for example a mirror's motion alters the electromagnetic field vacuum mode profiles, known as the dynamical Casimir effect (DCE) [8–11]. When the mirror moves at sufficiently high speeds, vacuum modes fail to adiabatically adjust to the mirror's new position, leading to a mismatch between the updated cavity modes and the original quantum state. This mismatch generates particle content, which, if detected, would correspond to photons spontaneously produced from highly non-perturbative spatial boundary condition changes.

The experimental observation of this phenomenon is a key objective for experiments at the interface of relativity and quantum theory because particle creation from the vacuum is also closely related to several fundamental yet unobserved phenomena such as Unruh and Hawking radiation [12–15], which have recently received more attention for experimental relevance [16, 17]. Such phenomena bridge several disciplines including quantum optics [18] and quantum field theory

in curved spacetime [19, 20], with applications to analogue gravity [21–23]. In this way, unambiguous confirmation of the local particle content due to highly non-perturbative boundary condition changes, would mark a major milestone in experiments in relativistic quantum physics.

The practicality of observing vacuum particle creation with a physical mirror has been debated, since a macroscopic object moving at the required relativistic speeds would endure immense mechanical stress, making the experiment highly impractical. In contrast, seminal experiments have successfully demonstrated particle creation from the vacuum without moving a mirror, instead generating observable photons by modulating the electric boundary conditions of a superconducting cavity [24] or using light in a superconducting metamaterial [?]. However, these experiments rely on resonant enhancement to produce the time-dependent boundary conditions in the DCE, where a single quantum of a driving field is converted into two entangled photons via a parametric process. Such particle creation processes are equivalently described as a parametric coupling between static cavity modes. Consequently, they cannot be interpreted as observations of particle content arising from a non-perturbative change in the boundary conditions—one that significantly alters the photonic cavity's spatial mode profile as originally proposed by Moore [8] (in our case splitting the photonic cavity into two). In contrast, the authors of Ref. [25] proposed to use a rapidly slammed mirror in a photonic cavity to generate local particles associated with spatial sub-regions of the vacuum. Such an experiment would access vacuum particle creation from non-perturbative boundary condition changes. However, this has remained far out of experimental reach due to the extremely high speed at which the mirror needs to be inserted in the cavity.

In parallel, atomic arrays are at the forefront of modern quantum physics, with transformative applications in quantum computing, quantum simulation, quantum sensing and metrology [26–32]. Specifically, sub-wavelength atomic arrays have

* germain.tobar@fysik.su.se

† magdalena.zych@fysik.su.se

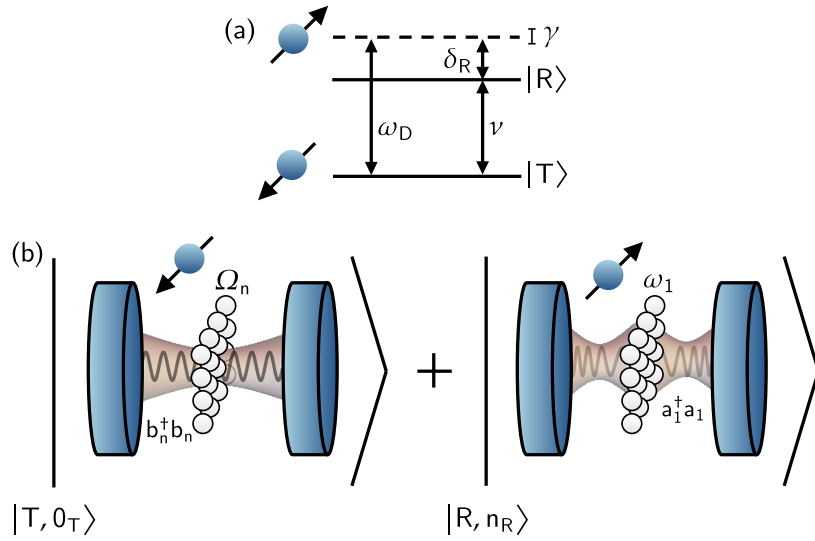


FIG. 1: (a) When the reflectivity of the two-dimensional atomic array changes, it leads to particle creation from the vacuum. This vacuum-induced effect causes a frequency shift, denoted by δ_R , in the transition frequency ν of the control atom. The shift occurs when the control atom is driven by an external field with drive frequency ω_D . As we show in this work, the frequency shift can be much larger than the linewidth γ of the control atom. (b) A quantum metasurface acts as a quantum-controlled mirror within a photonic cavity, where dynamical superpositions of reflective ($|R\rangle$) and transmissive ($|T\rangle$) states are created by driving the control Rydberg atom between its ground and excited state respectively. This dynamical superposition prepares superpositions of the cavity's boundary conditions, leading to observable frequency shifts of the control atom. These effects serve as a witness of particle content from entangled spatial sub-regions of the electromagnetic field vacuum, achievable without the need for classical rapid mirror motion. We note that while the array can be positioned at any place in the cavity, for practical realization we will consider it to be placed off-centre.

been proposed as platforms for realising a quantum metasurface [33], in which the atomic array can be toggled between dynamics of superpositions of transmissive ($|T\rangle$) and reflective ($|R\rangle$) states via control of the internal state of a single atom. Followed by proposals for employing them for atomic quantum operations [34, 35], their applicability in cavity set-ups is also receiving more attention, notably for their ability to provide confining mirrors in an optical cavity [36].

In this article, we propose a protocol to measure the particle content produced due to highly non-perturbative boundary condition changes using a quantum metasurface realised as a two-dimensional sub-wavelength atomic array [33]—that divides a photonic cavity. We show that vacuum particle creation due to highly non-perturbative boundary condition changes induces a measurable frequency shift in the control atom of the atomic array and is within reach of realistic albeit challenging near-term experiments. As we show here, by mapping particle creation onto the control atom's frequency shift, we sidestep the off-resonant suppression that occurs when the boundary condition changes on a timescale much shorter than the optical mode period (as in classical boundary-condition modulation). This will bring vacuum particle creation from non-perturbative boundary changes within experimental reach. Mapping particle creation onto this frequency shift also removes the need for rapid modulation of a classical mirror's reflectivity and instead enables quantum-controlled

switching, while at the same time generating coherent dynamics of superpositions of distinct photonic QED vacua. Observing the photon-induced frequency shift would constitute the first direct observation of vacuum particle creation in the sense of Moore's original work [8], i.e. driven by a non-perturbative change in the field's boundary conditions that partitions the electromagnetic vacuum into spatial sub-regions.

II. SUB-REGION PARTICLE CONTENT WITH A CLASSICAL MIRROR

We begin by outlining the theoretical framework for observing photon content from entangled spatial sub-regions of the vacuum with a rapidly introduced mirror, examined in Ref. [25]. Consider a photonic cavity of length L , where the mode functions satisfying the Klein-Gordon equation with Dirichlet boundary conditions are given by [25]:

$$U_n(x, t) = \frac{1}{\sqrt{L\Omega_n}} \sin\left(\frac{\pi n x}{L}\right) e^{-i\Omega_n t}, \quad (1)$$

where $\Omega_n = \frac{\pi n c}{L}$ are the resonance frequencies of the photonic cavity. The corresponding eigenstates are Fock states of the cavity's free Hamiltonian, $\hat{H} = \sum_{n=1}^{\infty} \Omega_n \hat{b}_n^\dagger \hat{b}_n$, where \hat{b}_n^\dagger and \hat{b}_n are creation and annihilation operators for mode n , satisfying commutation relations $[\hat{b}_n, \hat{b}_m^\dagger] = \delta_{nm}$. Now,

if a mirror is suddenly introduced at time $t = 0$ within the cavity, it alters the boundary conditions and introduces time-dependence into the Hamiltonian [25]:

$$\hat{H}(t) = \begin{cases} \sum_n \Omega_n \hat{b}_n^\dagger \hat{b}_n & t < 0 \\ \sum_m \omega_m \hat{a}_m^\dagger \hat{a}_m + \bar{\omega}_m \hat{a}_m^\dagger \hat{a}_m & t \geq 0, \end{cases} \quad (2)$$

where $\omega_m = \frac{\pi m}{r}$, $\bar{\omega}_m = \frac{\pi m}{\bar{r}}$ are the frequencies of the left and right sub-cavities of length r and $\bar{r} = L - r$ respectively. The mode functions of the sub-cavities have the form Eq. (1), with L replaced by r , \bar{r} , respectively. Together, the left and right sub-cavity modes span the same space as the full cavity, which means that the full cavity modes can be expressed in terms of sub-cavity modes. This relationship is given by the Bogoliubov relation between \hat{b}_n and the sub-cavity modes \hat{a}_j, \hat{a}_j [25]. In particular, the mode transformation for \hat{a}_j, \hat{a}_j takes the form,

$$\begin{aligned} \hat{a}_j &= \sum_{n=1}^{\infty} \left(\alpha_{jn} \hat{b}_n - \beta_{jn} \hat{b}_n^\dagger \right) \\ \hat{a}_j &= \sum_{n=1}^{\infty} \left(\bar{\alpha}_{jn} \hat{b}_n - \bar{\beta}_{jn} \hat{b}_n^\dagger \right), \end{aligned} \quad (3)$$

where the Bogoliubov coefficients are $\alpha_{jn} = \frac{j(-1)^j}{\sqrt{n}j\bar{a}\pi(n-\frac{j}{\bar{a}})} \sin(n\pi a)$ and $\beta_{jn} = \frac{j(-1)^j}{\sqrt{n}j\bar{a}\pi(n+\frac{j}{\bar{a}})} \sin(n\pi a)$ for the left sub-cavity, and $\bar{\alpha}_{jn} = \frac{-j}{\sqrt{n}j\bar{a}\pi(n-\frac{j}{\bar{a}})} \sin(n\pi a)$ and $\bar{\beta}_{jn} = \frac{-j}{\sqrt{n}j\bar{a}\pi(n+\frac{j}{\bar{a}})} \sin(n\pi a)$ for the right sub-cavity ($a = \frac{r}{L}$, $\bar{a} = \frac{\bar{r}}{L}$ is the ratio between the cavity lengths of the left and right sub-cavities to the global cavity respectively). These Bogoliubov coefficients quantify the mixing between the original modes and the new modes due to the mirror's sudden introduction. The nonzero $\beta_{jn}, \bar{\beta}_{jn}$ coefficients signify local photon content in the global vacuum, as the vacuum state of the global cavity is no longer empty in terms of the sub-cavity modes.

The average number of sub-cavity photons in mode i , evaluated in the vacuum state of the original global cavity, is given by $\langle \hat{n}_i(t) \rangle = \sum_{n \geq 1} |\beta_{in}|^2$. For the extremal case where the mirror is placed at the midpoint of the cavity, such that the ratio of the sub-cavity length to the global cavity length is $a = 0.5$, the number of created photons can reach values as high as $\langle \hat{n}_i(t) \rangle \simeq 0.05$. However, achieving this effect requires the spatial boundary conditions of the cavity to change non-perturbatively (in contrast to the experiments of Refs. [24?]) on a timescale faster than the free evolution of the cavity modes. It was suggested in [25] that a classical mirror with rapidly varying reflectivity could induce such fast and non-perturbative spatial boundary condition changes. Yet, this approach demands changes on the order of 10^{-14} s, which is far beyond feasible experimental capabilities due to the limitations of material response times [37].

III. THE QUANTUM-CONTROLLED PHOTONIC CAVITY

We previously saw that in order to observe particle content from the vacuum due to non-perturbative boundary condition changes with a classical metasurface, the transition from a transmissive to reflective metasurface would have to occur rapidly. In contrast, in this section we show how a quantum metasurface can make such particle content observable without the need for such rapid response times.

Our proposal places a sub-wavelength array of N neutral atoms close to the end of a single-mode Fabry-Perot cavity. As before, we denote the size of the global cavity by L and the left and right sub-cavities by r and \bar{r} respectively. We now assume that the atoms are situated close to the left mirror, such that the left sub-cavity is much smaller than the size of the global cavity, that is, $r \ll L$. Although the atoms could also be placed in the middle of the cavity (for which $r = \bar{r}$), we choose to work in this small sub-cavity regime in order to obtain a highly accurate analytical result, as well as maximise the frequency shift (in the $r \ll L$, the mode mis-match between the left sub-cavity mode and the global cavity mode functions is maximised leading to the most significant effect). As we demonstrate later, these results act as an order-of-magnitude estimate for other configurations, such as an array positioned close to the centre. We further note that for infinitely large L the QED vacuum can function as the global cavity. The relevant internal states of the array atoms are denoted the ground state $|g\rangle$, excited state $|e\rangle$ and Rydberg state $|r'\rangle$. When placed in a sub-wavelength configuration, such a two-dimensional array of atoms naturally acts as a near-perfect mirror for photons tuned to its collective $g \leftrightarrow e$ dipole transition. When a strong classical control field drives the $e \leftrightarrow r'$ transition, the array enters an EIT (electromagnetically-induced-transparency) regime: the destructive interference between the two excitation pathways opens a narrow transparency window, so the metasurface becomes almost loss-free and transmissive. The atom array therefore provides an implementation of a classical mirror in the cavity, which we considered in the previous section, depending on whether the EIT control beam is switched on or off. Implementing this sub-wavelength atom array in a cavity set-up remains the first step towards the implementation of our proposal.

To control the transmissive or reflective state of the atom array, we couple it to a neutral control atom. This was first proposed in Ref. [33]. By changing the state of the control atom, its interaction with the collective modes of the atom array tunes the array between transmissive and reflective states. When the control atom is excited to its own Rydberg state, the dipole-dipole (blockade) interaction shifts the $|r'\rangle$ level of every atom in the array, detuning the two-photon resonance and quenching EIT. As a result, any light injected into the cavity then sees the bare, highly reflective array, so the metasurface becomes a mirror for light resonant with the $g \leftrightarrow e$ dipole transition. Preparing the control atom in a quantum superposition of ground and Rydberg states therefore entangles the array with the control atom and realises a coherent superposition of the two macroscopic optical responses—transparent (EIT-enabled) and reflective. In other words, the state of the

control atom determines whether the atom array divides the global cavity into two sub-cavities or not.

We model the control atom as a qubit with control state $|R\rangle_c$ (for a reflective array) and $|T\rangle_c$ (for a transmissive array), as done in Ref. [33]. Such a sub-wavelength atom array tunable between quantised transmissive and reflective states has been observed experimentally in a free-space set-up rather than a cavity set-up in Ref. [38], albeit not yet extended to the coherent superpositions of Ref. [33].

The total Hamiltonian of the array-control-atom system can be expressed as

$$\hat{H} = \hat{H}_{\text{array}} + \hat{H}_{\text{free}} + \hat{U}_{\text{ryd}}, \quad (4)$$

where \hat{H}_{array} is the many body Hamiltonian of the array (see Appendix A), \hat{H}_{free} is the free Hamiltonian of the control atom, and $\hat{U}_{\text{ryd}} = \sum_i \hat{V}_i = \sum_i V_{ic} |R\rangle_i \langle R|_i \otimes |R\rangle_c \langle R|_c$ is the Rydberg-Rydberg interaction between the control atom and each atom in the array. This produces different dynamics of the array atoms conditioned on the quantum state of the control, essentially dynamics with or without the Rydberg interaction term. As a result, the permittivity of the atomic array, and therefore its reflectivity, produces a reflection coefficient dependent on the quantum state of the control. Previously, the permittivity of the array (which controls the reflectivity) was only computed when the control atom was in either the $|R\rangle_c$ or $|T\rangle_c$ state, inferring its extension to the case of a quantum-controlled permittivity [33]. In this work, we derive the reflectivity for exact dynamics of superposition states of $|R\rangle_c$ and $|T\rangle_c$, which is crucial for our proposal, and derive the relevant quantities, extending previous derivations. Henceforth, for ease of readability, we denote the extended collective mode of the many body state of the atomic array with the same quantum state as the control's quantum state. In this sense, one should be aware that the states $|R\rangle$ and $|T\rangle$ mathematically represent the full state of the control atom and the array on the joint Hilbert space $\mathcal{H}_{\text{control}} \otimes \mathcal{H}_{\text{array}}$ (and we have dropped the subscript “c” to indicate this).

So far, we have not yet considered the optical field in the cavity. When the atom array is tuned to the transmissive state $|T\rangle$, the global cavity supports standing modes of the optical field, which we denote by

$$\hat{H}_T = \sum_n \Omega_n \hat{b}_n^\dagger \hat{b}_n, \quad (5)$$

where Ω_n is the frequency of the supported global modes, \hat{b}_n , in the cavity. We show in Appendix B 4 that when the atom array is reflective to a set of frequencies in some reflectivity bandwidth Δ , the Hamiltonian describes now two sub-cavities, where the left sub-cavity confines the mode we denote \hat{a}_1 with frequency ω_1 , and the right sub-cavity, which confines a set of modes \hat{a}_k with frequencies $\bar{\omega}_k$; explicitly this Hamiltonian reads

$$\hat{H}_R = \sum_n \Omega_n \hat{b}_n^\dagger \hat{b}_n + \omega_1 \hat{a}_1^\dagger \hat{a}_1 + \sum_k \bar{\omega}_k \hat{a}_k^\dagger \hat{a}_k, \quad (6)$$

where as in the previous section \hat{b}_n refer to the global cavity modes of frequency Ω_n . This expression is valid in the

regime for which the global cavity length is much larger than the smaller sub-cavity length, $r \ll L$. In addition, we require the array to be reflective in a narrow frequency range, specifically, we require Δ , to be much smaller than the sub-cavity mode frequency spacing, *i.e* free spectral range (FSR): $\Delta \ll \omega_1$.

We now consider the case where the control atom is in a superposition of reflective and transmissive states, that is, $|\psi\rangle = (c_R |R\rangle + c_T |T\rangle)$. By linearity, the cavity Hamiltonian conditioned on the control's quantum state is

$$\hat{H}_{\text{cav}} = \hat{H}_T \otimes |T\rangle \langle T| + \hat{H}_R \otimes |R\rangle \langle R|, \quad (7)$$

which we derive through a quantum-control state-dependent interaction of the atomic array with the quantised field modes, starting from the microscopic QED interaction $\hat{H}_{\text{int}} = \hat{\mathbf{E}}(\mathbf{x}) \cdot \hat{\mathbf{P}}(\mathbf{x})$ in Appendix B. Here, \hat{H}_T is the global cavity Hamiltonian of Eq. (5) and it appears in \hat{H}_{cav} conditioned on the control being in the transmissive state. \hat{H}_R represents the reflective Hamiltonian, given in Eq. (6), and it appears in \hat{H}_{cav} conditioned on the control being in the reflective state. We re-iterate that this is valid in the regime for which the global cavity length is much larger than the sub-cavity length $r \ll L$, and the array is reflective in a narrow frequency range, $\Delta \ll \omega_1$.

Finally, we consider the mechanism by which the control atom is driven from the transmissive $|T\rangle$ state to the reflective $|R\rangle$ state. In the full dynamics, the control atom cannot be switched from $|T\rangle$ to $|R\rangle$ instantaneously; the corresponding drive Hamiltonian between such orthogonal states reads:

$$\hat{H}_{\text{switch}} = g (|T\rangle \langle R| e^{i\omega_D t} + \text{h.c.}) \quad (8)$$

Here, g corresponds to the Rabi coupling strength of the control atom with an incident drive of frequency ω_D . The term \hat{H}_{switch} thus describes how the control atom can drive transitions between the transmissive and reflective cavity states. The full Hamiltonian of the atom, cavity and control atom is $\hat{H} = \hat{H}_{\text{cav}} + \hat{H}_{\text{switch}} + \hat{H}_{\text{free}}$, where the free Hamiltonian of the control atom can be explicitly written as

$$\hat{H}_{\text{free}} = \frac{\hbar\nu}{2} (|R\rangle \langle R| - |T\rangle \langle T|), \quad (9)$$

where the transition frequency between the two relevant states is denoted ν .

IV. OBSERVING SUB-REGION PARTICLE CONTENT WITH A QUANTUM METASURFACE

The quantum-controlled coupling of the electromagnetic field energy to the control atom causes the vacuum state of the field to contain non-zero particle content. This, in turn, re-normalises the energy levels of the control atom. Our goal is to derive an analytic estimate of this frequency shift of the control atom due to vacuum particle content, arising from the change of the array's reflectivity, *i.e.* the appearance of a mirror in the cavity.

The effect of the local particle content of the cavity vacuum can be best understood by considering the form of the free Hamiltonian of the atom and the cavity, $\hat{H}_{\text{cav}} + \hat{H}_{\text{free}}$. This expression can be reorganised to emphasize how the control system's energy levels depend on the metasurface response and thus on the modes of the photonic cavity,

$$\begin{aligned} & \hat{H}_{\text{cav}} + \hat{H}_{\text{free}} \\ &= \left(\hat{H}_R + \frac{\hbar\nu}{2} \right) \otimes |R\rangle\langle R| + \left(\hat{H}_T - \frac{\hbar\nu}{2} \right) \otimes |T\rangle\langle T|, \end{aligned}$$

where $\hat{H}_R = \hat{H}_T + \omega_1 \hat{a}_1^\dagger \hat{a}_1 + \sum_k \bar{\omega}_k \hat{a}_k^\dagger \hat{a}_k$, as in Eq. (6), where it becomes clear that the energy levels of the control atom are renormalised by the distinct energy contributions from the global and sub-cavities, described by \hat{H}_T and \hat{H}_R respectively. The frequency shift depicted in Fig. 1 (δ_R), can thus be interpreted as a shift in the atom's resonance frequency, which is caused by the differing energy states of these two cavity configurations. As we will discuss further, this shift arises due to the sub-cavity having non-zero particle content for the global cavity vacuum state in the fast-switching regime (boundary condition changes on time-scales comparable to or much faster than the frequency of the optical mode $\tau_g \gtrsim \frac{1}{\omega_1}$), and non-zero particle creation in the slow switching regime (timescales much smaller than the free-evolution of the optical modes).

In order to further understand the frequency shift, we convert H_{switch} into the interaction picture with respect to $\hat{H}_{\text{cav}} + \hat{H}_{\text{free}}$, where the unitary evolution of the system, up to first order in g is

$$\hat{U}_I^{(1)} = \hat{\mathbb{I}} - ig \int_0^t dt' \left(e^{i\hat{H}_R t'} |R\rangle\langle T| e^{-i(\hat{H}_T + \delta)t'} + \text{h.c.} \right), \quad (10)$$

where $\delta = \nu - \omega_D$ is the detuning between the laser frequency and the control atom transition. Starting from an initial vacuum state of the global cavity $|0_T\rangle$ and the state of the control atom for which the metasurface is transmissive $|T\rangle$, the probability to measure the control atom in the reflective state $|R\rangle$ becomes (considering a weak drive $g \ll \omega_1$, where we recall that ω_1 is the frequency of the fundamental mode of the sub-cavity):

$$\begin{aligned} P_R &= 4(gt)^2 \left\langle \text{sinc}^2 \left(\frac{1}{2} \left(\delta + \omega_1 \hat{a}_1^\dagger \hat{a}_1 + \sum_n \Omega_n \hat{b}_n^\dagger \hat{b}_n \right) t \right) \right\rangle \\ &\simeq 4(gt)^2 \text{sinc}^2 \left(\frac{1}{2} (\delta + \delta_R) t \right), \end{aligned} \quad (11)$$

where the expectation value is taken with respect to the field state after the switch, and \hat{a}_1 , \hat{b}_n represent the fundamental sub-cavity and global mode operators respectively, and δ_R is an analytical estimate of the frequency shift due to the particle content created from a time-dependent boundary condition change. In order to observe particle content, we now focus on two distinct regimes where the atom array is switched from transmissive to reflective.

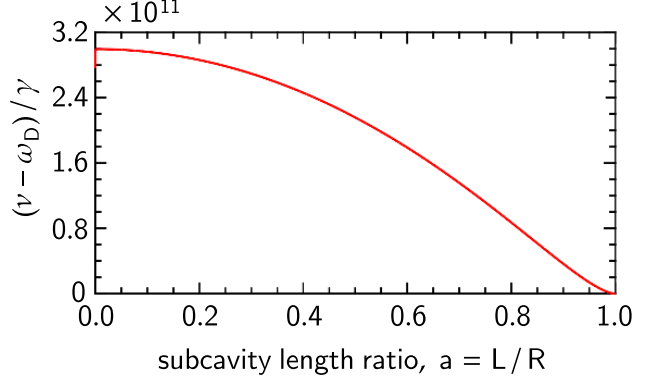


FIG. 2: Analytical estimate for the frequency shift as a function of the ratio of the left sub-cavity length to the global cavity length given in Eq. (13). The asymmetry in the frequency shift arises because the mirror only reflects a single frequency - higher order modes have a comparatively negligible contribution, leaving only the contribution from the fundamental mode which has this characteristic curve.

A. Slow-switching

In the most experimentally relevant regime where the array is switched from transmissive to reflective on a timescale comparable to the excited-state linewidth (Γ_e) of the array atoms, with $\tau_e \sim 1/\Gamma_e$, the photon content arises from the time-dependent reflectivity of the array. As the Hamiltonian changes from $\hat{H}_T \rightarrow \hat{H}_R$, the reflectivity coefficient varies in time and the initial vacuum state of the field is no longer the vacuum of the instantaneous Hamiltonian. This deformation of the vacuum, driven by a highly non-perturbative change in the boundary conditions, produces spatially localised photons from the vacuum, with a photon number of order $n \sim (\Gamma_e/\omega_1)^2$ (see Appendix B 3). In this regime, the sub-cavity field evolves into $|\beta_R\rangle = |0\rangle + \frac{\Gamma_e}{\omega_1} |1\rangle + \mathcal{O}((\frac{\Gamma_e}{\omega_1})^2)$, which is a coherent state of amplitude $\frac{\Gamma_e}{\omega_1}$. This change of state arises due to the time-dependent boundary as the array switches from the EIT Dark state to a highly reflective state, as outlined in Appendix. A 2, leading to the non-zero particle content,

$$\langle \beta_R | \hat{a}_1^\dagger \hat{a}_1 | \beta_R \rangle = |\beta_R|^2 \geq 0, \quad (12)$$

Importantly, the relevant particle content is controlled by the finite switching rate (or ramp time) and is vanishing in the adiabatic (infinitely slow switching) limit—relative to the sudden-switch value, as derived in Appendix B 3.

In summary, this protocol constitutes a novel approach to observe vacuum-particle production due to non-perturbative boundary condition changes. This is achievable with this system due to the scaling enhancement by the factor ω_1 for measuring particle content compared to the noise threshold, as can be extrapolated from Eq. (11), compared to classical mirror modulation of Ref. [39]. To see this explicitly, for the control atom's linewidth γ - the vacuum frequency shift compared to

the linewidth is $\frac{\omega_1 |\beta_R|^2}{\gamma}$.

B. Fast-switching

In the fast switching regime (which requires improvements beyond the current state-of-the-art), the expectation value in Eq. (11) is taken with respect to $|0_T\rangle$, as the field state remains unchanged before and after the switch, and $\delta_R = \sum_n \omega_1 |\beta_{1,n}|^2$ is an analytical estimate of the frequency shift due to the sub-region particle content in this fast switching regime (see Appendix C1 for a derivation in the rotating frame of \hat{H}_R , after expanding sub-cavity modes in terms of global cavity modes with a Bogoliubov transformation or multi-mode squeezing operation [40]). This particle content is plotted as a function of the ratio of the global and sub-cavity length in Fig. 2. We present the derivation of the above perturbative expression for the transition probability in Appendix C2. From Eq. (11), it is apparent that the presence of photons in the sub-cavity with respect to the global cavity vacuum state,

$$\langle 0_T | \hat{a}_1^\dagger \hat{a}_1 | 0_T \rangle = \sum_n |\beta_{1n}|^2 \geq 0, \quad (13)$$

produces a frequency shift of the control atom. This analytical expression for the frequency shift is exact in the $r \ll L$ regime, while providing an order-of-magnitude estimate when the atomic array is positioned elsewhere in the cavity. This particle content in Eq. (13) that produces the characteristic frequency shift corresponds to the case of ideal rapid switching, which requires Purcell-enhanced-linewidths several orders of magnitude beyond state-of-the-art [41] for the exact protocol described in this section to work (as we detail further in section V).

C. Extraction Protocol

The following protocol can be used to verify the predicted vacuum-induced frequency shift of the control atom in either the fast or slow switching regimes with the shifted frequency as outlined in Eq. (11). Firstly, the control atom is prepared in the transmissive state $|T\rangle$. Next, the control atom is pumped on-resonance with the control atom's un-renormalised transition frequency ν . In this case, due to the frequency shift from the presence of vacuum-photons, there will be a significantly reduced probability for the control atom to flip to the reflective state $|R\rangle$. If the smaller sub-cavity of length $r \ll L$ is then pumped on-resonance with sub-cavity mode \hat{a}_1 , the typical Lorentzian peak in the power spectrum of the output mode (at the frequency ω_1 of the mode \hat{a}_1) will not be observed. However, if the sub-cavity is pumped on-resonance with the re-normalised transition frequency $\nu' = \nu + \sum_n \omega_1 |\beta_{1,n}|^2$ (or $\nu' = \nu + \omega_1 |\beta_R|^2$ in the slow switching case), the array will flip to the reflective state (due to incident photons to the cavity being resonant with the $|g\rangle \rightarrow |e\rangle$ transition for the control atom), and the output power spectrum will have a peak

at ω_1 , as expected given that the reflective Hamiltonian \hat{H}_R forms standing waves at the frequency ω_1 . This average intensity will be suppressed by $g^2/(g^2 + \delta^2)$ for a drive detuned from the transition frequency by δ , as demonstrated in Appendix C4 (the average reflected number of photons will be weighted by the probability for the array to be in the reflective state). For a drive detuned by $\delta \sim 0.1$ Hz, and Rabi coupling strengths as weak as $g \sim 10^{-14} \omega_1$, the suppression of the average intensity is by a factor of $1 - 10^{-4}$ compared to the intensity in the sub-cavity on-resonance. The dominant contribution to all particle-content-induced frequency shifts comes from the left (and smaller) sub-cavity. The off-resonant nature of the drive Hamiltonian with the cavity frequency ensures the photon content produced can only be explained by the boundary condition change rather than photons pumped into the cavity. If set-up enables direct access to the control atom, the frequency shift can further be measured through measurements on the control atom directly. We further note that frequency shifts smaller than the linewidth can be resolved in this manner through many repetitions of the experiment, but this will require a large number of runs of the experiment (a single-shot Rabi drive and measurement of the cavity power spectrum will generally not be sufficient) - assuming \sqrt{N} precision, then $N = 10^{10}$ iterations will give down to sub-Hz precision - achievable with existing technology.

V. OBSERVABLE FREQUENCY-SHIFT MAGNITUDE AND SCALING

A. Array Parameters

For the protocol described in Section IV to lead to the successful observation of such vacuum particle content, several experimental requirements must be met. Here we discuss the parameter requirements of the atomic array system in order to witness the discussed effects in the fast and in the slow switching regimes.

In order to observe either the vacuum's unperturbed particle content or slow-switching particle creation from strongly non-perturbative boundary changes, our protocol requires that the control atom acts as the quantum degree of freedom setting the cavity boundary condition. In order to achieve this, it is crucial that the Rydberg blockade of the control atom reaches each atom in the array, such that driving the control atom into its Rydberg state switches off the transparency through the Rydberg blockade as in Ref. [33]. Although switching the control atom between states takes $O(1/g)$ time, in the reflective branch of the superposition the energy levels of the array atoms shift within the light-crossing time. After this, the atom array's reflectivity switches on, changing from the EIT dark-state transmissivity to a reflective state determined by the array properties—notably the excited state linewidth Γ_e and the EIT control-beam coupling strength Ω_p . We classify four regimes of relevance with varying experimental feasibility as summarised in Table I.

To capture the different physical behaviours of the system, we analyse three distinct parameter regimes in a full time-

Switching regime	Required parameters	Switching parameter	Switching time-scale	Measured Frequency Shift
Slow non-parametric	$\frac{\Omega_p^2}{\Gamma_e V} \gg 1$	Γ_e	10 ns (1 ns)	0.1 Hz (10^{-16})
Slow non-parametric enhanced	$\frac{\Omega_p^2}{\Gamma_e V} \gg 1$	Γ_e	0.001 ns (1 ns)	100 Hz (10^{-13})
Slow parametric	$\frac{\Omega_p^2}{\Gamma_e V} \ll 1$	Ω_p	ps (ns)	1 Hz (10^{-14})
Fast non-parametric	$\frac{\Omega_p^2}{\Gamma_e V} \gg 1$	Γ_e	fs (0.1 ns)	10^{11} Hz (10^{-5})

TABLE I: Table of parameters for switching time-scales of the atomic array’s reflectivity needed to produce a particle-content-induced frequency shift in the final column, with comparison to state-of-the-art switching times in brackets in the fourth column. Standard atom linewidths are on the order of $\Gamma_e \sim 10$ MHz, with an assumed two order of magnitude enhancement of $\Gamma_e \sim 1000$ MHz. Extreme Purcell-enhanced linewidths are on the order of $\Gamma_e \sim$ THz as stated in the main text. The EIT control beam coupling strength for standard parameters is on the order of $\Omega_p \sim$ MHz. For strong EIT control beam coupling strengths $\Omega_p \sim 10$ GHz, one can undertake slow switching parametric particle creation as highlighted in the third row, while typical MHz strengths would suppress it to Hz-scale frequency shifts. The different regimes can be accessed by initialising the control atom in its ground state, and driving transitions to the excited state, the relative strength of the Rydberg interaction energy (V) in comparison to the EIT linewidth (second column) allows access to the distinct regimes. The last column quantifies the frequency shift and converts it into a fractional frequency shift.

domain treatment of the reflectivity switch, presented in Appendix A. We firstly focus here on the first regime, which is based on the standard Rydberg blockade mechanism for switching on the reflectivity. This is the same physical process used in the experiment of Ref. [38], where strong interactions between Rydberg excitations prevent multiple atoms enabled the switch of the collective mode of the array from transmissive to reflective correlated with the state of the quantum-control.

In the limit where the Rydberg interaction strength is much larger than the effective EIT linewidth, Ω_p^2/Γ_r (with Ω_p the control-beam coupling strength and Γ_r the Rydberg decay rate), we find that the reflectivity does not turn on instantaneously. Instead, it rises on a timescale set by the excited-state linewidth. Physically, this means that the optical response of the array is limited by how quickly population can build up in the excited state. As a result, the system operates in the slow-switching regime discussed in Section IV A.

This slow switching leads to a small but finite frequency shift of the optical mode, which scales as $(\Gamma_e/\omega_1)^2$ (see Appendix B 3), where Γ_e is the excited-state linewidth and ω_1 is the mode frequency. The corresponding particle production in this regime is shown in the first row of Table I. Importantly, this shift can be significantly enhanced using Purcell-enhancement, bringing it into the kilohertz range (as indicated in the second line). The resulting timescale defines the central operating regime of this work and is crucial for enabling non-perturbative vacuum particle creation to be observed with near-term experimental technology.

The second regime of slow-switching parametric particle production, as given in Table I, line three, is that of small Rydberg interaction strengths compared to the EIT linewidth. We find that fast oscillations of low effective reflectivities (see Appendix A Figure 4), will enable the switching time to oscillate on the time-scale of the EIT control beam coupling strength Ω_p , which for typical EIT linewidths corresponds to a similar MHz switching rate. While accessible with near-term set-ups, this regime enables parametric particle production in the

global cavity akin to the experiments of Refs. [24?], i.e. the boundary condition change is perturbative reducing to parametric squeezing operation affecting the global cavity modes, as outlined in Appendix B 2.

The final regime given in Table I corresponds to the fast switching regime described in Section IV B, i.e. switching time-scales sufficiently fast compared to the time-scale for the free-evolution of the fundamental sub-cavity mode (2.5 fs for $\frac{\omega_1}{2\pi} \sim 400$ THz). The first of these non-adiabatic regimes would correspond to a Purcell-enhanced linewidth [41] by several orders of magnitude for the standard linewidth-limited switching of the first regime discussed above. In this way, if the Rydberg-blockade-induced energy shift is much larger than the EIT linewidth, if the array atom’s $|g\rangle \rightarrow |e\rangle$ transition has a radiatively enhanced linewidth by several orders of magnitude (as in the Purcell effect), the switching time-scale can approach the femto-second regime, as Purcell broadening of the linewidth will enhance the switching rate (see Appendix A 2). In this case, the protocol from Section IV can be used to extract the frequency shift, but will require an additional photonic cavity coupled to the array atoms (achievable with orthogonal modes) to radiatively enhance their linewidths. However, achieving the enhanced time-scales this fast is out of reach of near-term technology.

In order to quantitatively assess the magnitude of the reported particle-content-induced frequency shift in both the fast and slow-switching regimes, we now compare the magnitude of the frequency shift to the linewidth of the control atom. We assume a fundamental sub-cavity mode frequency on the order of 400 THz normalised to a control atom linewidth on the order of 10 kHz [42]. Our results demonstrate that for ideal, fast-switching (given in the last row of Table I), the shift in the transition frequency is on the order of 2.8% of the total transition frequency, but over 11 orders of magnitude larger than the linewidth (due to the Bogoliubov transformation contributing a frequency shift that is approximately 7% of the photonic cavity frequency, see Appendix C 1 for more details). The numbers for the frequency shift above are computed for

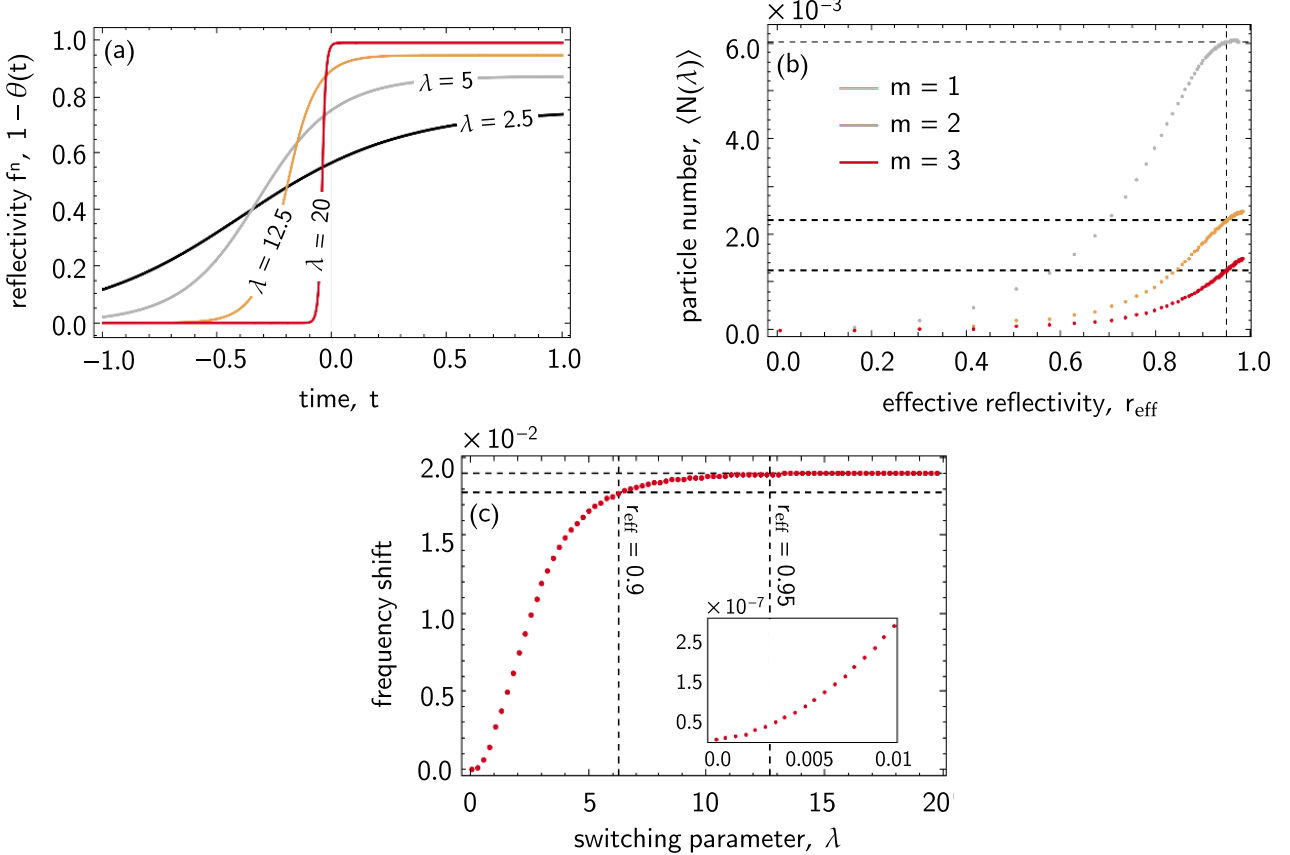


FIG. 3: (a) Plot of the switching profile $r(t) = 1 - \theta(t)$ as a function of time, where $r = 1$ corresponds to perfect reflection. The orange curve depicts an effective reflectivity $r_{\text{eff}} = 0.95$. (b) Plot of the particle content of the m th sub-cavity mode in the global vacuum state as a function of the effective reflectivity r_{eff} . We have plotted this difference for a cavity with walls at $x = \pm a/2$ with $a = 1$. The dashed lines correspond to $r_{\text{eff}} = 0.95$. (c) Plot of the estimated frequency shift re-normalised to the sub-cavity frequency ω_1 , $\frac{\delta\omega}{\omega_1} = \sum_n |\beta_{1,n}|^2$ obtained within our toy model, as a function of the switching parameter λ . The inset plots the frequency shift in the slow-switching regime corresponding to low effective reflectivities $r_{\text{eff}} \sim 10^{-4}$. Recall that λ serves a dual purpose: it determines both the proximity of the mirror's final state to perfect reflectivity and the speed at which the mirror is activated.

the case of ideal rapid switching (non-adiabatic boundary condition changes), which can be accessed in one of two central ways as summarised in Table I. As displayed, this large frequency shift requires either a significantly Purcell-enhanced linewidth for the atoms in the atomic array (specifically by four orders of magnitude, which is three orders of magnitude beyond state of the art for Purcell-enhanced linewidths [41]). In this case, the array's response time-scale is set by the EIT control beam strength Ω_p , leading to slow switching particle production. Alternatively, implementation can be completed in the fast-switching regime with the development of the quantum metasurface at microwave frequencies with superconducting artificial atoms, where such systems already have the parameters required for fast switching [43], or the development of a quantum metasurface at mm-wavelengths, which would require appropriate transduction for the read-out as proposed in Ref. [44].

In the slow switching regime, corresponding to the first two

parameter regimes discussed in this section (and given in the first three rows of Table I), we show that the particle content is suppressed by a factor proportional to the ratio $(\Gamma_e/\omega_1)^2$ (where Γ_e is time-scale for the reflectivity rise simulated in Appendix A 2), which corresponds to a frequency shift approximately an order of magnitude larger than the linewidth. This corroborates a simple toy model for a slowly switched mirror that yields a power law suppression of the produced particle content (see Fig. 3 and discussion below). More generally, the particle content created being proportional to $(\Gamma_e/\omega_1)^2$, once mapped onto a frequency shift on the control as per Eq. (10), gives an ω_1 factor enhancement of the signal above the linewidth of the control atom. This corresponds to an ω_1 factor scaling enhancement in the feasibility of witnessing such vacuum particle creation effects compared to the classical mirror modulation of Ref. [39]. This analysis demonstrates how the quantum-controlled mirror can provide a quantum advantage over classical boundary condition

changes for vacuum photon creation.

B. Atomic Species

We now consider the atom species required to fulfill the requirements just discussed. The numbers used to compute the change in the transition frequency are adapted from a state-of-art experimental system of ^{87}Rb sub-wavelength atom array that has potential for implementation of our proposed scheme [38], or alternatively with Yb atoms [45]. Specifically, we consider the following energy levels: $|g\rangle = |5\text{S}_{1/2}, F = 2, m_F = -2\rangle$ as the ground state and $|e\rangle = |5\text{P}_{3/2}, F = 3, m_F = -3\rangle$ as the excited state, resonating at $\omega_1/2\pi = 400$ THz. Accessing a fundamental mode of this frequency will require a cavity of order sub-micron length, specifically 375 nm long. While such a small cavity will increase the resonance line width by a factor proportional to $\frac{1}{r}$, this will not substantially reduce the power spectrum for such small resonators. For lattice spacing $a \simeq 0.2\lambda_1$, where λ_1 is the wavelength of the fundamental sub-cavity mode, (also achievable with Yb atoms), corresponding to 150 nm, the array achieves perfect reflectivity [45], making it reflective to modes near ω_1 . For sub-cavity linewidth $\kappa \ll \omega_1$, this frequency would be the only supported mode, allowing the atomic array to serve as one end of a sub-cavity, similar to that proposed in Ref. [36]. We consider the Rydberg control atom to also be a ^{87}Rb atom, but consider the ground state of the ancilla control to be $|g'\rangle = |5\text{S}_{1/2}, F = 1, m_F = -1\rangle$, with Rydberg state $|r_P\rangle = |44\text{P}_{3/2}, m_J = 3/2\rangle$, which has a transition at $\nu/2\pi = 1000$ THz, with achievable Rabi drive strengths of $g/2\pi \sim 1$ MHz [38], and assume an ancilla linewidth on the order of $\gamma/2\pi \simeq 10$ kHz [42]. Therefore, for this arrangement of a two-dimensional atomic array, if the array is $\frac{\lambda_1}{2} \simeq 375$ nm from one end of the cavity producing a sub-cavity with frequency ω_1 , the ideal frequency shift of the control atom will be $\delta_R \sim$ THz (also corresponding to that resolvable with ultra-fast optics), with the fast oscillation of low reflectivities and slow-switching case an order of magnitude larger than the linewidth. The main limiting factor in extending the switchable mirror demonstrated in Ref. [38] to the formation of coherent dynamics of quantum superpositions of transmissive and reflective states is increasing the decay time of the control atom from $T_1 \simeq 27$ μs demonstrated in Ref. [38] to become on the order of $T_1 \simeq 100$ μs , as demonstrated in Ref. [46].

We further require that the control atom be able to be driven between the ground and excited state in a coherent manner. In order to achieve this, for the control-atom parameters considered here, and practical optical cavity Q -factors κ on the order of 10^8 or larger, the co-operativity is above unity for coherent oscillations. For example, using $\frac{g}{2\pi} \sim 10^6$ Hz, $\frac{\kappa}{2\pi} \sim 10^8$, and $\frac{\gamma}{2\pi} \sim 10^4$ Hz (where γ is the linewidth of the control atom), gives well above unity for the Rabi-drive enhanced co-operativity, allowing coherent Rabi oscillations for the control atom. Moreover, such a small decay rate κ ensures that photons in the reflective branch of the superposition survive long enough to produce a measurable frequency shift.

VI. NOISE AND IMPERFECTIONS

Two main sources of imperfections are thermal motion of the atomic array, and imperfect reflectivity. Regarding the former, assuming an atomic array that has a collective motional DoF cooled to the quantum ground state, the magnitude of thermal motion of the array will be on the order of its zero-point motion [47]. In sub-wavelength atom arrays the Lambe-Dicke parameter η quantifies the spatial spread of an individual atom [48]. For example, the standard deviation of position divided by λ_0 (wave-length of the incident light) is equal to $\eta/2\pi$ for the vibrational state. It is given by $\eta = k_0\sqrt{\hbar/(2m\omega_t)}$, where ω_t is the trap frequency, which is typically on the order of several hundred kHz, and k_0 is the wavenumber of the incident light. To reflect optical light as we consider here, these parameters imply a positional spread on the order of 10 nm, much smaller than the cavity length.

The reflectivity of the array is not perfect. To account for this, we utilise a toy model in Appendix C3 (see also Ref. [49]) to compute the particle content produced by a smoothly switched reflective mirror that divides a Dirichlet cavity. Importantly, as the dominant particle content for the single frequency mirror in the main text is due to the fundamental sub-cavity mode, we can apply the corrections for the imperfect reflectivity for the fundamental sub-cavity mode to the single frequency mirror used in the main text. The switching of the mirror is determined by a one-parameter family of time-dependent profiles, $\theta(t) = (2/\pi)\tan^{-1}((1 + e^{-\lambda t})/(\lambda))$. This choice of $\theta(t)$ is such that solutions to the cavity Klein-Gordon equation smoothly interpolate between transmissive in the asymptotic past, to partially (i.e. imperfectly) reflective in the asymptotic future. The “effective reflectivity” $r_{\text{eff}} = 1 - \theta(\infty)$ (i.e. the closeness of the mirror’s end state to a Dirichlet boundary) is controlled by the parameter λ , which also quantifies how quickly the mirror is switched on, see Fig. 3(a). As shown in Fig. 3, both the particle content of the sub-cavity modes and the estimated frequency shift induced on the control atom are only slightly suppressed (see Fig. 3(b)-(c)) for experimentally expected reflectivities $r_{\text{eff}} \sim 0.95$ [33]. Even in the slow-switching regime for which $\lambda \sim 10^{-3}$ ($r_{\text{eff}} \sim 10^{-4}$), corresponding to a μs switching timescale (see Appendix C3), the particle content is only suppressed by six orders of magnitude, which would still correspond to a signal larger than the linewidth. For standard array parameters, this is the relevant experimental regime, as we detail in Appendix A2. We find that the frequency shift in this slow-switching regime follows a similar power law scaling at short times to the full model of the atom array’s response function (see inset to Fig. 3(c)).

VII. DISCUSSION

Let us begin by examining the historical context of the dynamical Casimir effect (DCE), first proposed by Moore as particle production resulting from a moving mirror at the boundary of a one-dimensional photonic cavity [8]. Revisiting this original setting allows us to later compare modern experi-

ments—and our proposal—to early theoretical considerations. In Moore's work, the effect arises from a time-dependent boundary condition: the photonic cavity length changing from r to R due to the motion of one mirror. The resulting particle creation, particularly in the non-adiabatic regime, is closely related to that studied in Ref. [25]. However, Moore's scheme required the mirror to move at relativistic speeds for particle creation to reach detectable levels. At lower velocities, the effect is strongly suppressed, placing such experiments well beyond practical reach. This limitation was later addressed by exploiting parametric resonance, which enables a resonant enhancement of particle production [50–52]. Such a mechanism forms the basis of the first breakthrough experimental observations of the DCE, achieved using time-dependent electric fields as boundary conditions rather than physically moving mirrors [24?]. Parametric coupling of fixed cavity modes also underlies recent proposals that involve mechanical acceleration of mechanical membranes [53], or acceleration radiation from vibrating atoms [54] or similar resonant amplification processes arising from internal system dynamics [55–59], as well as the generation of photons from a blue-detuned pulse in optomechanical set-ups [60].

The parametrically amplified DCE experiments and proposals discussed above therefore could not probe particle creation from non-perturbative boundary condition changes across distinct spatial regions, as proposed in Ref. [25], or originally analysed by Moore [8]. Instead, all proposals and observations to date have relied on parametric coupling between pairs of cavity modes induced by the mirror's motion, with boundary conditions modifying the photonic mode only

perturbatively. Consequently, the photonic mode profiles remain effectively unchanged and the dynamics reduce to an effective parametric interaction between unperturbed cavity modes.

The parametric generation of photons from the mechanical motion of a mirror boundary of a photonic cavity is a procedure commonly employed in quantum optomechanics [60], and we outline the connection further in Appendix D. In contrast, the particle creation described in Ref. [25], and originally considered in Ref. [8] is fundamentally distinct: it involves detecting photons arising from entangled, spatially distinct regions of the electromagnetic vacuum, as the field re-adjust to non-perturbative changes in the boundary conditions. This process, which underpins the particle creation phenomena considered by Moore [8] arises due to a mismatch between the local and global modes of a quantum field integrated across a non-perturbative change in boundary condition for the field modes, which is the same feature that is behind effects such as Hawking and Unruh radiation. In the present work, this feature is present in both the fast and slow switching regime - the total particle creation integrated across the switch arises due to a highly non-perturbative boundary condition change affecting the cavity mode profiles and involves the generation of entangled pairs of particles across the two spatially localised sub-cavities. In this way, the experimental implementation of our proposal will unlock the first experimental demonstration of the particle creation due to fundamentally split photonic mode structures as was originally considered in the original dynamical Casimir effect [8].

Appendix A: Quantum-controlled atom array response from the microscopic interactions

Here, we derive the permittivity of the atomic array, and therefore its reflectivity conditioned on the state of the control atom. This will enable us to compute the array's response time, and eventually derive the quantum-controlled interaction Hamiltonian which forms the core model for this work, Eq. (7) in the main text. This builds from the theory of Refs. [33, 45], but goes beyond these works by deriving the dynamics and reflectivity of the atomic array conditioned on the quantum state of the control atom, and simulating the time-domain dynamics given initialisation in an EIT Dark state of the atomic array.

1. Response function from the microscopic interactions for semi-classical fields

The permittivity $\alpha_{\mathbf{k}}$ of the atom array for a collective mode of momentum \mathbf{k} is derived in Ref. [33] from $\hat{H}_{\text{array}} + \hat{U}_{\text{ryd}}$ to be proportional to the coherence (the off-diagonal elements of the collective mode $\rho_{eg,\mathbf{k}}$) as

$$\alpha_{\mathbf{k}} = \frac{|\mu|^2}{\hbar} \frac{\rho_{eg,\mathbf{k}}}{\Omega_{\mathbf{k}}}, \quad (\text{A1})$$

where $|\mu|$ is the dipole moment of the array atoms, and $\Omega_{\mathbf{k}}$ is the coupling strength to the incident field, and simplifying with the spontaneous emission rate, $\gamma = \frac{|\mu|^2 8\pi^2}{3\lambda^3 \epsilon_0 \hbar}$ (where λ is the wavelength of resonance of the array atoms on the $|g\rangle \rightarrow |e\rangle$ transition), such that the permittivity becomes:

$$\alpha_{\mathbf{k}} = \frac{3\epsilon_0 \gamma \lambda^3}{8\pi^2} \frac{\rho_{eg,\mathbf{k}}}{\Omega_{\mathbf{k}}} \quad (\text{A2})$$

with the vacuum permittivity ϵ_0 . The permittivity is related to the reflection coefficient $S_{\mathbf{k}}$ through [61],

$$S_{\mathbf{k}} = i\pi \left(\frac{\lambda}{a}\right)^2 \frac{\alpha_{\mathbf{k}}}{\epsilon_0 \lambda^3}, \quad (\text{A3})$$

where a is the spacing between atoms in the array. Now, using the co-operative corrections to the linewidth as $\Gamma_{\mathbf{k}} + \gamma = \gamma \frac{3}{4\pi} \left(\frac{\lambda}{a}\right)^2$ [61], this simplifies to be:

$$S_{\mathbf{k}} = i \frac{(\Gamma_{\mathbf{k}} + \gamma)}{2} \frac{\rho_{eg,\mathbf{k}}}{\Omega_{\mathbf{k}}}. \quad (\text{A4})$$

We henceforth drop the subscript \mathbf{k} , leaving reference to a specific collective mode of the array of momentum \mathbf{k} implicit. This directly quantifies the reflection coefficient for incident light through scattering theory:

$$\mathbf{E} = \left[e^{ikz} + S e^{ik|z|} \right] \mathbf{E}_0, \quad (\text{A5})$$

where S quantifies the reflection coefficient for the incident electromagnetic field \mathbf{E}_0 . This establishes a Dirichlet boundary condition for the electromagnetic field at $z = 0$ when $S = -1$, as the field vanishes in the region $z > 0$ (while the expressions we give are for the right-moving fields, analogous relations hold for the left-moving ones, incident from the opposite side of the boundary at $z = 0$). In this way, we can directly relate the coherence to a reflection coefficient for the electromagnetic field, thereby quantifying the response function and reflectivity of the field through the coherence [33].

The total Hamiltonian of the array-control atom system can be expressed as

$$\hat{H} = \hat{H}_{\text{array}} + \hbar\omega_0 \hat{\sigma}_z^c + \hat{U}_{\text{ryd}}, \quad (\text{A6})$$

where \hat{H}_{array} is the Hamiltonian of the array used in Ref. [33] to derive the permittivity and therefore reflectivity of the atomic array to incident radiation. We now explicitly write the Hamiltonian of the array atoms with the EIT control beam on as

$$\hat{H}_{\text{array}} = -\Delta |r\rangle\langle r| - \Omega_{\mathbf{k}}(|e\rangle\langle g| + |g\rangle\langle e|) - \Omega_p(|e\rangle\langle r| + |r\rangle\langle e|), \quad (\text{A7})$$

where Δ is the single photon detuning. This quantum-mechanical derivation of the array coherence accounts for the Rydberg interaction energy \hat{U}_{ryd} , which shifts the atoms' energy levels and thereby modifies the coherence—and hence the effective permittivity—of the atomic array, tuning it from highly reflective to transparent.

Here, starting from the total Hamiltonian in Eq. (A9), we can define a permittivity conditioned on the control being in the transmissive or reflective state, thereby deriving the action of such a quantum-controlled atomic array on the cavity modes as a quantum-controlled potential-well, applied in Sec. B 2. In order to see this, we use the Rydberg-Rydberg interaction Hamiltonian, between the i th atom in the array and the control atom as

$$\hat{V}_i = V_{ic} |R\rangle_i \langle R|_i \otimes |R\rangle_c \langle R|_c, \quad (\text{A8})$$

with $\hat{U}_{\text{ryd}} = \sum_i \hat{V}_i$. If we multiply the remainder of the Hamiltonian in Eq. (A7), by the identity matrix on the control atom's Hilbert space, we can thus re-arrange the Hamiltonian modeling the microscopic interaction between the control atom and each atom in the array as

$$\hat{H} = \left(\hat{H}_{\text{array}} + \hbar\omega_0 \hat{\sigma}_z^c + \sum_i V_{ic} |R\rangle_i \langle R|_i \right) \otimes |R\rangle_c \langle R|_c + \left(\hat{H}_{\text{array}} + \hbar\omega_0 \hat{\sigma}_z^c \right) \otimes |T\rangle_c \langle T|_c, \quad (\text{A9})$$

and re-derive the equations of motion for the amplitudes of the array atoms — obtaining one set of the equations used in Ref. [33] for each of the control atom's orthogonal quantum states, $|R\rangle$ and $|T\rangle$. Denoting c_g^j , $c_{e,\vec{k}}^j$ and $c_{r,\vec{k}}^j$ as the probability amplitude of the array atoms to be in the $|g\rangle$, $|e\rangle$ and $|r\rangle$ states respectively, conditioned on the control atom's quantum state $j \in \{T, R\}$, we have

$$\begin{bmatrix} \dot{c}_g^j \\ \dot{c}_r^j \\ \dot{c}_e^j \end{bmatrix} = \begin{bmatrix} 0 & 0 & i\Omega_{\mathbf{k}}^* \\ 0 & -\Gamma_r & i\Omega_p^* \\ i\Omega_{\mathbf{k}} & i\Omega_p & -\Gamma_e \end{bmatrix} \begin{bmatrix} c_g^j \\ c_r^j \\ c_e^j \end{bmatrix}, \quad (\text{A10})$$

with $V^T = 0$, and $\Gamma_r = [(\gamma_r/2 - i(\delta_r + V^j))]$, and $\Gamma_e = [(\gamma + \Gamma_{\mathbf{k}})/2 - i(\delta - \Delta_{\mathbf{k}})]$. In Ref. [33], these equations of motion are solved to compute the coherence $\rho_{eg,\mathbf{k}} = c_g^* c_{e,\mathbf{k}}$ in the steady state, through $\alpha(\mathbf{k}) = \frac{|\mu|^2}{\hbar} \frac{\rho_{eg,\mathbf{k}}}{\Omega_{\mathbf{k}}}$ as above, and therefore the reflectivity is:

$$S^j(\omega) = \frac{i(\gamma + \Gamma_{\mathbf{k}})(\delta_r + V^j)}{-i(\delta_r + V^j)(\gamma + \Gamma_{\mathbf{k}} - 2i(\delta - \Delta)) + 2|\Omega_p|^2}, \quad (\text{A11})$$

where here $\delta = \omega_{eg} - \omega$ is the detuning of the light from the atomic resonance, and γ denotes the radiative lifetime of the state $|e\rangle$. It is standard now to apply this control-dependent reflectivity derived for weak incident classical fields, carries over to weak incident quantum fields in the absence of non-linearities.

2. Time-domain Switching dynamics

a. Initial Conditions

In this section, we now solve for the EIT time-domain dynamics given initialisation of the collective mode in an EIT Dark state. Here, Δ and Γ are the co-operative corrections to δ and γ arising from dipole-dipole interactions, and $\delta_r = \omega_{rg} - \omega_p - \omega$, is the two-photon detuning. In order to model the time-domain dynamics, we consider that the Hamiltonian in Eq. (A7) has the EIT dark state as an eigenstate:

$$|D\rangle = \cos \theta |g\rangle - \sin \theta |r\rangle, \quad (\text{A12})$$

with $\tan(\theta) = \frac{\Omega_k}{\Omega_p}$, for small θ , this dark state becomes

$$|D\rangle \simeq |g\rangle - \frac{\Omega_k}{\Omega_p} |r\rangle. \quad (\text{A13})$$

With this quantum-controlled EIT model, we can now undertake detailed modeling for the various regimes of the array's response function. In the main text, there are four regimes discussed for the scaling of the switching of the array's reflectivity which are presented as the core results. These different regimes can be accessed depending on the initial state of the array, as well as the strength of the Rydberg interaction as compared to the EIT linewidth $\Gamma_{\text{EIT}} = \frac{\Omega_p^2}{\Gamma_e}$.

Next, we solve for the time-domain dynamics of the reflectivity function of Eq. (A10), we first check that in the absence of a Rydberg shift, we qualitatively re-obtain similar dynamics that was recently derived in Ref. [62] for the transmissivity (the imaginary component of the susceptibility), without extending to the full four-level model of Ref. [62]. Next, we compute the rise of the coherence and, therefore, of the reflectivity out of the initial EIT dark state after a switch-on of the Rydberg interaction (resulting in the energy level shift of the array atoms). We find that for typical array parameters (as discussed in Section V), the rise of the coherence, and therefore the susceptibility (and therefore the transmission and reflection coefficients), change on the time-scale given by the linewidth of the array atoms, as simulated in Fig. 4 (a).

b. Regime I

The first regime discussed in the main text—corresponding to linewidth-limited slow switching—is obtained by solving the system of ODEs in Eq. (A10) under the assumption that the system is initially prepared in the dark state. The time-domain solution is $\vec{c}(t) = P e^{\vec{D}t} P^{-1} \vec{c}(0)$, which describes the transition from the dark state to the reflective state of the atomic array. For the standard array parameters considered in Section V, where the Rydberg interaction strength is much larger than the EIT linewidth ($V^R \gg \Gamma_{\text{EIT}}$), the susceptibility switches on over nanosecond timescales. This places the system firmly in the slow-switching regime, in which the field modes adjust adiabatically to the changing boundary conditions, with deviations from the vacuum state arising only through non-adiabatic corrections to the adiabatic theorem.

This slow-switching behaviour is evident in the time-dependent reflectivity, which at short times grows exponentially with rates set by the eigenvalues of Eq. (A10), and in practice is governed by the linewidth Γ_e . Although the switching is slow in the adiabatic sense, at early times the reflectivity still rises sharply from zero, leading to a transient low-reflectivity “slam” that generates measurable photon content and an associated frequency shift. The total effect can be obtained by integrating these non-adiabatic corrections over the full switching interval, as computed in Section B 3. This process corresponds to vacuum particle creation driven by highly non-perturbative changes in the boundary conditions, forcing the vacuum to reorganize into split cavity modes—a significant step beyond previous dynamical Casimir experiments and closer to the original effect proposed by Moore [8].

Accordingly, for these standard array parameters we model the reflectivity as $r(t - t_0) = 1 - \exp[-\kappa \Gamma_e (t - t_0)]$, where t_0 is the switch-on time and κ is extracted from the full ODE solution shown in Fig. 4. This form captures a switching time of order a few inverse linewidths and closely matches the slow-switching toy model, particularly the short-time power-law scaling of the reflectivity. Finally, although these parameters allow for particle creation through non-adiabatic corrections to the adiabatic theorem with standard array parameters, we emphasize that increasing the atomic linewidth by several orders of magnitude would push the system into the fast-switching regime, where accessing the ideal frequency shift for rapid switching becomes possible.

c. Regime II

The second regime discussed in the main text corresponds to initialising in the EIT Dark state, and examining the dynamics for $V^R \ll \Gamma_{\text{EIT}}$. The system exhibits oscillations of low reflectivities on a time scale proportional to the EIT probe beam

strength $\approx 0.01\Omega_p$. For EIT probe beams such that $\Omega_p/2\pi \sim \text{MHz} - 10 \text{ GHz}$, such switching to low reflectivities as depicted in Fig. 4 (b) is realistic, enabling parametric vacuum particle content production to be observed (as for such low reflectivities this corresponds to a parametric particle creation effect, albeit with perturbative boundary condition changes). For the third regime, the non-adiabatic particle content can be accessed if the regime for which $V \gg \Gamma_{\text{EIT}}$ is accessed, and Purcell-enhanced linewidths are used that are several orders of magnitude beyond the state of the art.

d. Regime III

The final regime involves using strong EIT control beams on the order of $\Omega_p/2\pi \sim 100 \text{ GHz}$, initiating in a highly reflective state, and we simulate the array's susceptibility to flip to rapidly oscillate about zero reflectivity on time-scales proportional to Ω_p . This would enable switching on the time-scale of a tenth of a picosecond, which would reach within a factor of 50 of the optical frequency (and therefore obtain experimental relevance for the fast-switching regime). In order to access this regime, it is imperative that the EIT control beam reach this 100 GHz strength - albeit this is a very experimentally challenging regime for a driving strength on the $|e\rangle \rightarrow |r\rangle$ transition for the array atoms.

3. Response function from the microscopic interactions for quantum fields

The susceptibility derived above—evaluated for a fixed state of the control atom—remains applicable to quantum fields as long as the light–matter coupling is linear. In our setting, the probe corresponds to the low-amplitude excitations of the cavity field, for which the mean linear response of the atoms is the same for a classical drive and for weak coherent or thermal quantum states. It follows that the array response obtained for a weak classical probe carries over to weak Gaussian quantum probes (with vacuum as the zero-mean limit). We now derive this explicitly starting from the full QED interaction,

$$\hat{H}_{\text{int}} = \hat{\mathbf{E}}(\mathbf{x}, t) \cdot \hat{\mathbf{P}}(\mathbf{x}, t), \quad (\text{A14})$$

between quantum field modes and the atomic array.

The coupling of the quantized electric field to atomic sources in free space is most naturally treated using a Green's function formalism. In this approach, the atoms appear as localized sources in the equations of motion for the field. The positive frequency component of the polarization operator can be written as a sum over point-like atomic sources,

$$\hat{\mathbf{P}}(\mathbf{x}, t) \simeq \sum_l \hat{d}^l(t) \delta^l(\mathbf{x} - \mathbf{x}_l), \quad (\text{A15})$$

where $\hat{d}^l(t) = \mu_{\text{ge}}^l \hat{\sigma}_{\text{ge}}^l(t)$, is the dipole operator of the l -th atom and μ_{ge}^l its dipole matrix element. We further restrict to a single longitudinally polarised mode with finite transverse area A , so that the transverse delta function is replaced by $\delta(\mathbf{x}^\perp) = 1/A$. In this formulation, the resulting wave equation, the atomic array appears as a delta-function barrier in the equations of motion for the field, a representation that we will exploit in Section (B 2).

As discussed above, the response function derived in this framework applies in the regime of linear response for quantum fields. A closely related formulation for a linear drive has been analysed in Ref. [45]. To make the connection explicit, and following Ref. [36], we now examine the corresponding input–output relation for the re-radiated field. As previously explained, the response function previously derived applies in the regime of interactions with quantum fields in the regime of linear response and has been commented on for a linear drive in Ref. [45]. In order to derive this explicitly, following Ref. [36], the Heisenberg equations of motion for the field if the probe beam on the $|g\rangle \rightarrow |e\rangle$ transition is promoted to a quantum field, (Here, $\mathbf{G}^*(\mathbf{r}, \mathbf{r}_j, \omega)$ is the dyadic Green's for free space) are

$$\begin{aligned} \dot{\hat{\mathbf{E}}}(\mathbf{r}, \omega) = & -i\omega \hat{\mathbf{E}}(\mathbf{r}, \omega) + \frac{\omega_0^2}{c^2} \sqrt{\frac{1}{\pi\hbar\epsilon_0} \text{Im}\{\epsilon(\mathbf{r}, \omega)\}} \\ & \times \sum_{l=1}^N \mathbf{G}^*(\mathbf{r}, \mathbf{r}_l, \omega) \cdot \mu \hat{\sigma}_l^-(t), \end{aligned} \quad (\text{A16})$$

(now replacing $\hat{\sigma}_{\text{ge}}^l(t) \rightarrow \hat{\sigma}_l^-$, and assuming identical dipole moments $\mu = \mu_{\text{ge}}^l$) which corresponds to the electric field in the global cavity interacting with the array atoms via the Dyadic Green's function (for a large global cavity we can use the Dyadic Green's function for free-space)

$$G(\mathbf{r}_i, \mathbf{r}_j) = \frac{e^{ikr}}{4\pi r} \left[\left(1 + \frac{ikr - 1}{k^2 r^2} \right) + \frac{3 - 3ikr - k^2 r^2}{k^2 r^2} \frac{|r_d|^2}{r^2} \right]. \quad (\text{A17})$$

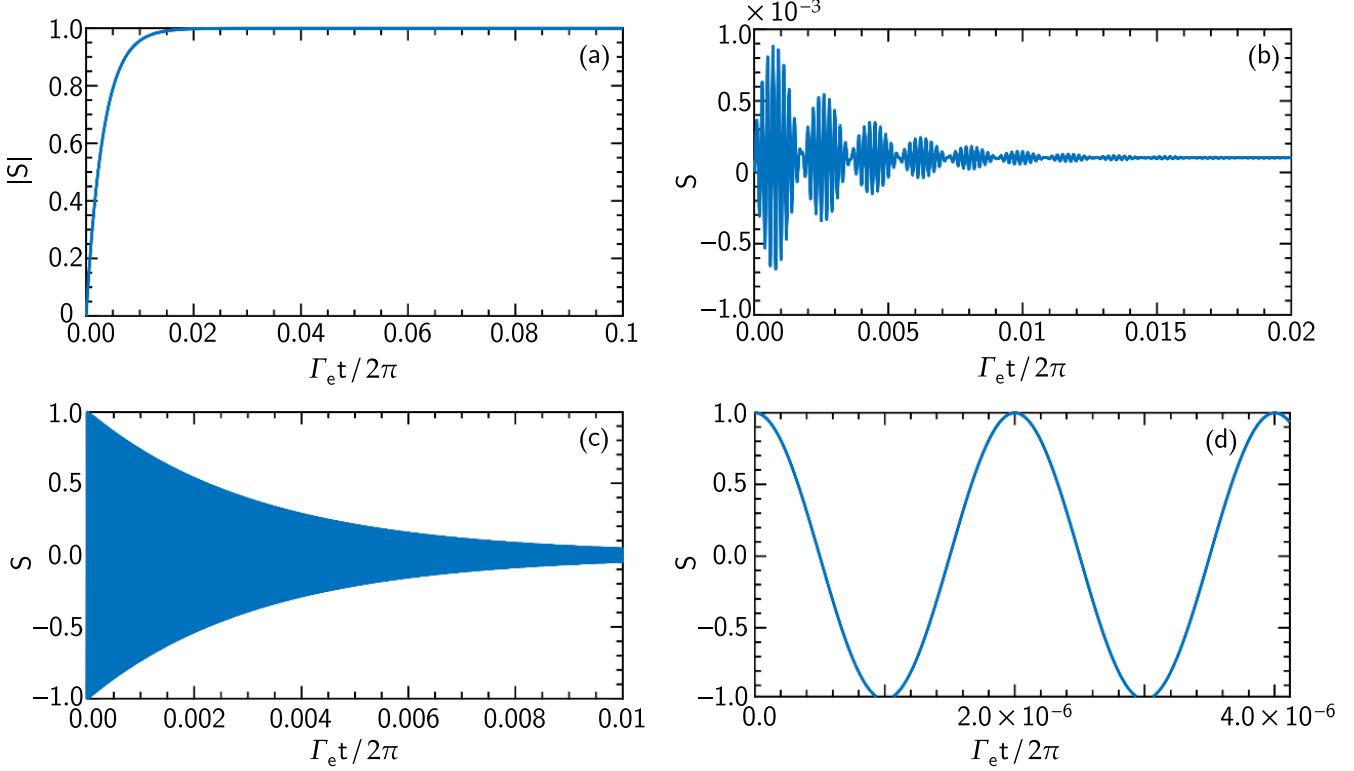


FIG. 4: (a) Time-dependence of the reflectivity of the atomic array initialised in the EIT dark state, after a speed of light switch on of the Rydberg potential energy V^R . The time is renormalised to the linewidth, with $\Omega_p = 10\Gamma_e$, $V^R = 10^5\Gamma_e$, $\Gamma_e = \Gamma_r$. (b) Time-dependence of the reflectivity of the atomic array initialised in the EIT dark state, after a speed of light switch on of the Rydberg potential energy V^R . The time is renormalised to the linewidth, with $\Omega_p = 10^4\Gamma_e$, $V^R = 10^3\Gamma_e$, $\Gamma_e = \Gamma_r$. In this regime, the Rydberg interaction is not strong enough to switch the array to near unit reflectivity. However, fast oscillations are observed before reaching the steady state, on a time-scale proportional to Ω_p . (c) Time-dependence of the reflectivity after initialising in the highly reflective state with the Rydberg shift on in the regime $V^R \gg \frac{\Omega_p^2}{\Gamma_r}$, and a speed of light switch-off of the Rydberg interaction energy, in this regime for which $\Omega_p = 10^4\Gamma_e \gg \Gamma_e$, fast oscillations are observed on the time-scale Ω_p , with a decay envelope on the time-scale of the linewidth. (d) Inset into the fast oscillations displayed in (c). Code for the simulations is attached as an ancillary file. Scaling the EIT control beam coupling strength all the way down to MHz coupling strengths yields the same qualitative behaviour in (b) and (c) with slower oscillation speeds, this enables parametric particle production in this regime going from MHz – GHz scale oscillation speeds.

From this, the reflection co-efficient follows to be (after projecting the Green's function onto the output electric field mode, and conversion to the collective mode of the dipoles) [63],

$$\hat{r}_j = \frac{i}{2k_0} \frac{\omega_0^2 \sqrt{N}}{Na^2 \epsilon_0 c^2} \mu^k \hat{\sigma}_j^-, \quad (\text{A18})$$

where-as in the semi-classical calculation we define control-conditioned dynamics with the label $j \in \{T, R\}$, promoting this quantity to an operator that quantifies the reflected electric field conditioned on the quantum state of the control. We use this as the time-domain expression for the reflectivity of the atomic array, indeed matching the formula derived using a classical field drive as derived below. Now, extending the Heisenberg-Langevin equations to a three-level system, and converting to be in terms of the collective mode operators we obtain the dynamics of the polarisation operator from the interaction Hamiltonian in Eq. (A14):

$$\dot{\hat{\sigma}}_R^- = -i\sqrt{N} \mu^k \hat{E}(\mathbf{r}, t) (\hat{\sigma}_{ee}^k - \hat{\sigma}_{gg}^k) + \sqrt{N} \left(i\omega_e - \frac{\Gamma_e}{2} \right) \hat{\sigma}_R^- + \sqrt{2\Gamma_e} \hat{P}_{in}(t), \quad (\text{A19})$$

where we have assumed a loss-less field mode of the EM field. The input noise operator satisfies the following correlation

function relations (for negligible thermal excitation):

$$\hat{S}_{\text{in}}(t) = \sqrt{2\Gamma_e} \hat{P}_{\text{in}}(t), \quad \langle \hat{S}_{\text{in}}(t) \rangle = 0, \quad \langle \hat{P}_{\text{in}}(t) \hat{P}_{\text{in}}^\dagger(t') \rangle \approx \delta(t - t'), \quad (\text{A20})$$

as the fermionic correlations match the relation for bosons in the limit of negligible thermal occupation [64]. Equation (A19) corresponds to the simplified Heisenberg–Langevin equations under the following assumptions: (i) the atoms are initialised in the EIT dark state up to $\mathcal{O}((\Omega_k/\Omega_p)^2)$; and (ii) in the reflective (blockaded) branch the EIT control beam is shifted off resonance by the Rydberg interaction, so its coupling can be neglected (equivalently, in the rotating frame of the $|r\rangle$ -transition the Rydberg-shifted term is counter-rotating and is dropped), it can be checked that the re-including this term and initialising the atom in the EIT Dark state of Eq. (A13) the coherence and therefore the reflectivity remains zero for all times, using $\hat{\sigma}_{ee} - \hat{\sigma}_{gg} \approx \rho_{ee} - \rho_{gg} \approx -1$ (weak-probe limit). We use that the positive frequency component of the electric field at the barrier is

$$\hat{E}(\mathbf{r}, t) = g_q \hat{a} f(\mathbf{r}, t), \quad (\text{A21})$$

where $f(\mathbf{r}, t)$ is the standing-wave mode function while the collective coupling carries the usual \sqrt{N} enhancement. With these identifications, the reflectivity coefficient defined in Eq. (A18) is equivalent to the one obtained from the semi-classical derivation in Eq. (A3), using again the weak-probe limit. The first Heisenberg–Langevin equation in (A19) then has the Fourier-domain solution,

$$\hat{\sigma}_R^-(\omega) = -i \frac{\sqrt{N} \mu^k \mathbf{E}(\omega)}{i(\omega - \omega_e) - \frac{\Gamma_e}{2}}, \quad (\text{A22})$$

substituting this result into the reflection coefficient derived above and working in the near-resonant regime $\omega - \omega_e \ll \frac{\Gamma_e}{2}$ we recover exactly the same coefficient as in Refs. [33, 45]. The same result may be also obtained by modelling the array as an infinitesimally thin atomic sheet with areal density N_0 and susceptibility $\chi = \frac{N_0 \alpha_k}{\epsilon_0}$, where, $\alpha_k = \frac{|\mu|^2}{\hbar} \frac{\rho_{eg,k}}{\Omega_k}$. For a large 2D array ($N \gg 1$) with lattice spacing a , the area density is $N_0 = \frac{N}{N a^2} = \frac{1}{a^2}$. This provides a third derivation of the same reflection coefficient, now written explicitly for the interaction with weak quantum fields. Directly integrating the initial equation for the coherence (and assuming close to resonance with the atomic transition frequency), up to noise terms we obtain,

$$\hat{\sigma}_R^-(t) = +i\sqrt{N} \mu^k E_q \int_0^t d\tau f(\mathbf{r}, \tau) \left(\hat{a}(\tau) e^{((t-\tau)(i\Delta_e - \frac{\Gamma_e}{2}))} + \hat{a}^\dagger(\tau) e^{(-(t-\tau)(i\Delta_e + i\omega_c + \frac{\Gamma_e}{2}))} \right) + \text{noise term}, \quad (\text{A23})$$

where $f(\mathbf{r}, t)$ is, in general, time dependent (we take $t = 0$ to be the switching time), and Δ_e is the detuning from the atomic resonance frequency. From here on, we drop the control-conditioned subscript and leave the control dependence implicit: the linewidth-limited polarisation operator refers to the reflective branch, while no barrier refers to the transmissive branch. Coupling to higher-order cavity modes is suppressed by their detuning set by the free spectral range (FSR), so we retain only the single cavity mode that lies within the array’s reflectivity bandwidth. Finally, assuming the mode function does not change appreciably during the switch, we may treat $f(\mathbf{r}, t) \approx f(\mathbf{r})$ and simplify the expression by neglecting counter-rotating terms.

$$\hat{\mathbf{P}}(t) = \frac{2i(\mu^k)^2 \hat{E}^+(t)}{\Gamma_e} \left(1 - \exp\left(-\left(\frac{\Gamma_e t}{2}\right)\right) \right) + \sqrt{2\Gamma_e} \int_0^t d\tau e^{-(i\Delta_e + \frac{\Gamma_e}{2})(t-\tau)} \hat{P}_{\text{in}}(\tau), \quad (\text{A24})$$

when this is substituted into the wave equation for the electric field, this produces a barrier term with the same reflection coefficient given in Eq. (A18), supplemented with an in-homogeneous noisy source term.

Appendix B: Quantum-controlled Hamiltonian

In this section, we now apply the state-dependent reflectivity of the previous section to derive the energy distribution of the field modes conditioned on the quantum-state of the control.

1. QED back-action

The Langevin equation considered in the previous section, or wave equations for the quantised field can be extended to control-conditioned dynamics in a straight-forward manner as in Eq. (A9), but now explicitly extended to the back and forth

dynamics of quantised field modes interacting with the array, rather than a weak classical field. In order to see this, we take the wave equation for the quantised electric field that can be derived from the Heisenberg equation of motion for the field operators:

$$\begin{aligned}\dot{\hat{\mathbf{P}}}(t) &= -\left(\frac{\Gamma_e}{2} + i\Delta_e\right)\hat{\mathbf{P}}(t) + \sqrt{N}\mu^{\mathbf{k}}\hat{\mathbf{E}}(t) + \sqrt{2\Gamma_e}\hat{P}_{in}(t), \\ \partial_x^2\hat{\mathbf{E}} - \partial_t^2\hat{\mathbf{E}} &= \frac{1}{\varepsilon_0}\partial_t^2\hat{\mathbf{P}}(t).\end{aligned}\quad (\text{B1})$$

We first integrate the polarisation equation, assuming harmonic electric-field modes. In addition, we restrict to a single cavity mode that is significantly modified by the barrier, and we place the barrier near a node of the two sub-cavity modes (as discussed in Sec. B 2). Under these assumptions, Eq. (A24) gives the solution for the polarisation field. Substituting this solution into the equation for the quantised electric field, and neglecting sub-leading terms suppressed by the linewidth, we obtain the following equations of motion for the instantaneous cavity-mode amplitudes within the array's reflectivity bandwidth. Contributions from modes outside this bandwidth are off-resonant and are therefore suppressed by their frequency detuning:

$$\partial_x^2 f(x, t) + k_0^2 f(x, t) = \frac{r(t)k_0}{2} f(x, t) \delta(x - r_x). \quad (\text{B2})$$

where r is the reflection co-efficient of Eq. (A18) (the pre-factor of the scattered electric field operator) now given in terms of this linewidth limited rise from zero reflectivity (restricting as considered earlier to a longitudinally polarised sinusoidal mode of the electric field with finite transverse area on the order of $A = Na^2$), where N is the number of atoms and a is the lattice spacing. Now, breaking up the electric field into an incident and scattered field, we obtain the barrier term as $g(t) = \frac{k_0 r(t)}{1+r(t)}$ for the reflected field, which as expected reproduces the dynamics of the interaction Hamiltonian of the electric field with an imperfectly reflective barrier considered in Ref. [65]. We use this in the next section while simplifying into a scalar field model. Crucially this re-normalises the electric field equation of motion into an oscillator with time-dependent frequency given by the time-dependent reflection co-efficient that produces the characteristic non-adiabatic particle creation corrections on the order of $\frac{\Gamma_e}{\omega_1}$.

If we now consider the Heisenberg evolution of observables of the photonic field $O(\hat{a})$, we obtain

$$\dot{O}(\hat{a}) = -i\omega_c[\hat{a}^\dagger\hat{a}, O(\hat{a})] + g_q[(\hat{a} + \hat{a}^\dagger), O(\hat{a})](\hat{\sigma}_{\text{ge}}^{\mathbf{k}}(t) + \hat{\sigma}_{\text{ge}}^{\mathbf{k}}(t)^\dagger), \quad (\text{B3})$$

expanding in terms of the integrated form in Eq. (A23) for the $\hat{\sigma}_{\text{ge}}^{\mathbf{k}}(t)$ and $\hat{\sigma}_{\text{ge}}^{\mathbf{k}}(t)^\dagger$ pieces, we find two pieces that contribute, the rotating terms produce frequency shifts, while the counter-rotating terms produce squeezing co-efficients of the order of $\frac{\Gamma_e}{\omega_1}$ for the cavity mode when evaluated with respect to the input state. In general, the back-substitution of the polarisation operator defines a re-normalised time-dependent mode for the electromagnetic field that we solve for in the next sections (and adds a connection piece that generates finite particle creation).

2. Quantum-Controlled Reflectivity Mapped to Scalar Field Theory

Here we derive the Hamiltonian for the photonic cavity conditioned on the quantum-control variable, which forms Eq. (7) in the main text. We take as a starting point, the Hamiltonian density of a free scalar field $\phi(x, t)$, with the understanding as in Ref. [25] that it can be used as a model for a single polarisation of the electromagnetic field confined to an optical cavity. This can be seen explicitly by associating the electromagnetic vector potential in 1-D to be $A_x \rightarrow \frac{\phi}{\sqrt{\epsilon_0}}$, $E_x \rightarrow \frac{\dot{\phi}}{\sqrt{\epsilon_0}}$ in which case the QED Hamiltonian reduces to:

$$\mathcal{H} = \frac{1}{2} \left[(\dot{\phi})^2 + (\partial_x \phi)^2 \right], \quad (\text{B4})$$

and impose Dirichlet boundary conditions $\phi(0) = \phi(L) = 0$, upon quantisation, as in Section A for the array atoms. We supplement this free field Hamiltonian density with the quantum-controlled version of the scattering relation in Eq. (A5). Here, the effect is implemented as a delta function potential with coupling strength conditioned on the quantum state of the control:

$$\hat{\mathcal{H}}_{\text{int}} = g\delta(x - r)\hat{\phi}_{\Delta}^2 \otimes |R\rangle_c\langle R|_c + \hat{I} \otimes |T\rangle_c\langle T|_c. \quad (\text{B5})$$

Here, $\hat{\phi}_{\Delta}$ denotes the component of the field within the array's reflectivity bandwidth. In the transmissive branch, there is no coupling between light and the atomic array because the array is in an EIT dark state (Appendix A9). This delta function barrier is equivalent to the back-and-forth action derived in Appendix A, as using this delta function interaction, produces the same equations of motion, i.e. the same wave equation that we consider below but for the electric field. In essence, it is equivalent

to eliminating the dynamics of the atomic array by substituting the back-reflected electric field and provides the same equation of motions as outlined in the previous section when restricting to the dynamics of a single transverse component of the electric field. We use it to model the quantum-controlled matrix element derived in Appendix A9, since it produces a similar discontinuity in the field mode functions to that found for the electric field modes in Appendix C3.

We next aim to construct the full quantum-controlled Hamiltonian density. Firstly, we multiply the free Hamiltonian density in Eq. (B4), by identity on the field DoF times identity on the control Hilbert space $\hat{I} \otimes \hat{I}_c$, where $\hat{I}_c = |R\rangle_c \langle R|_c + |T\rangle_c \langle T|_c$. Modelling the presence of a mirror as a delta function potential for the field, conditioned on the state of the quantum-control as in Eq. (B5), allows us to construct the following Hamiltonian density for the quantum field conditioned on the state of the quantum control system:

$$\hat{\mathcal{H}} = \left(\frac{1}{2} \left[\left(\frac{d}{dt} \hat{\phi} \right)^2 + (\partial_x \hat{\phi})^2 \right] + g\delta(x-r)\hat{\phi}_\Delta^2 \right) \otimes |R\rangle_c \langle R|_c + \left(\frac{1}{2} \left[\left(\frac{d}{dt} \hat{\phi} \right)^2 + (\partial_x \hat{\phi})^2 \right] \right) \otimes |T\rangle_c \langle T|_c. \quad (\text{B6})$$

This quantum-controlled model for the presence or absence of a barrier also follows directly from linearity given the distinct energy distributions with and without the presence of the barrier in the two branches of the superposition. To proceed with simplifying this Hamiltonian, we use the following expansion of the field in terms of mode functions: $\hat{\phi}(x, t) = \sum_{m=1}^{\infty} f_m(x) \hat{b}_m e^{-i\Omega_m t} + \text{h.c.}$. In the transmissive branch of the superposition, the mode functions $f_m(x)$ are the standard global cavity mode functions in Eq. (1) of the main text, such that quantisation in the transmissive branch through substitution of this expansion in Eq. (B4) leads to the standard Hamiltonian of the global cavity modes:

$$\hat{H}_T = \sum_n \Omega_n \hat{b}_n^\dagger \hat{b}_n, \quad (\text{B7})$$

where $\Omega_n = \frac{\pi n}{L}$. In the reflective branch of the superposition, we consider only a single mode $f_0(x)$ to fall within the reflectivity bandwidth and is made discontinuous through the barrier, we thus take as an ansatz

$$f_0(x) = \begin{cases} A \sin(kx), & 0 < x < r \\ B \sin(k(L-x)) & r < x < L, \end{cases} \quad (\text{B8})$$

The delta function potential and a single reflected frequency imply the following equations of motion (for the instant-time mode functions) in the reflective branch of the Hamiltonian in Eq. (B6) for a general time-dependent barrier strength g :

$$\begin{aligned} f_0''(x) + k^2 f_0(x) &= -2g\delta(x-r)f_0(x), \\ \tilde{f}_n''(x) + k_n^2 \tilde{f}_n(x) &= 0, \end{aligned} \quad (\text{B9})$$

where the second line is for $n \geq 1$ (the global cavity modes, with the lowest order mode subtracted as in Eq. (B13)). The delta function potential here driving the fundamental mode matches the dynamics derived in the previous section for the atomic array back-reacting on the electric field, after associating g with the wave-number multiplied by the reflection co-efficient in Eq. (A18) or the solution for polarisation operator in the electric field wave equation of Eq. (A24), expanding in terms of instantaneous mode functions and neglecting the connection terms (negligible for small spatial deformations of the mode functions) as outlined in the previous section. Essentially we match the strength of g to the reflection co-efficient of the previous section. Integrating this from $r^+ = r - \epsilon$ to $r^- = r + \epsilon$, and taking $\epsilon \rightarrow 0$ gives the following condition on the mode function in the array's reflectivity band-width (up to surface terms):

$$f_0'(r^+) - f_0'(r^-) = 2g f_0(r). \quad (\text{B10})$$

If $g \rightarrow 0$, then this derivative jump and continuity of f_1 implies algebraically that Eq. (B8) reduces to the form in Eq. (B13), while for sufficiently large g , they decouple into two completely independent sub-cavities, with boundary condition $f_1(0) = f_1(R) = f_1(r) = 0$. In order to see this, we note that continuity and the jump condition in Eq. (B10), respectively imply

$$\begin{aligned} A \sin(kr) &= B \sin(k(L-r)) \\ \sin(kL) + \frac{2g}{k} \sin(kr) \sin(k(L-r)) &= 0. \end{aligned} \quad (\text{B11})$$

This implies that for perfect transmission, such that $g = 0$, we have $\sin(kL) = 0$, implying the mode functions patch together, and can form standing waves of the global cavity. For $g \gg k$, such that there is a strong barrier, the product term in the second equation needs to be correspondingly small which can be satisfied by either of the sine-functions vanishing sufficiently fast at the boundary. We thus expand about $kr = \pi + \epsilon_L$, and $k(L-r) = m\pi + \epsilon_R$, which for small ϵ_R, ϵ_L , gives $\sin(kr) \propto -\frac{k}{2g}$, $\sin(k(L-r)) \propto -\frac{k}{2g}$, which for $g \rightarrow \infty$ that gives standing modes with an additional Dirichlet boundary

condition at $x = r$ for the left and right sub-cavities, decoupling the cavities into independent sub-systems. More generally the second line in Eq. (B11) implies two sets of solutions that require either $\sin(kr) \rightarrow 0$, $\sin(k(L-r)) \rightarrow 0$ as $g \rightarrow \infty$, by the continuity equation, one implies the other. In this limit, one of the consistent normalisation constants for the global cavity mode in Eq. (B8) are exactly the Bogoliubov co-efficients for the N -th global cavity mode in terms of the fundamental left sub-cavity mode and right sub-cavity mode such that both have the same frequency of the global cavity, and it can be seen that the global mode deforms into the normal modes of the membrane in the middle Hamiltonian with a near unit reflectivity barrier.

We now expand the field operators in terms of the mode functions. Here \hat{a}_1 and \hat{a}_k are left and right sub-cavity modes with the array's reflectivity band-width. Next, the total field and its conjugate momentum can be expressed as (in the Schrodinger picture)

$$\hat{\phi} = \sum_{n=0}^{\infty} f_n(x) \hat{q}_n, \quad \hat{\Pi} = \sum_{n=0}^{\infty} f_n(x) \hat{p}_n, \quad (\text{B12})$$

where $\hat{q}_n = \frac{1}{\sqrt{2}}(\hat{b}_n^\dagger + \hat{b}_n)$, $\hat{p}_n = -i\sqrt{\frac{1}{2}}(\hat{b}_n - \hat{b}_n^\dagger)$, for $n \geq 1$, with

$$\tilde{f}_n(x) = f_n(x) - (f_n | u_1) u_1(x) - (f_n | u_1^*) u_1^*(x) - (f_n | \bar{u}_k) \bar{u}_k + (f_n | \bar{u}_k^*) \bar{u}_k^\dagger. \quad (\text{B13})$$

Here $f_n(x) \rightarrow \tilde{f}_n(x)$ (for $n \geq 1$) define the mode functions for the modified global cavity modes $\hat{\tilde{b}}_n$, and $f_n(x)$ are the unperturbed global cavity modes for $n \geq 1$, given in Eq. (1) of the main text, while $u_1(x) = \frac{\theta(r-x)}{\sqrt{r\omega_1}} \sin\left(\frac{\pi x}{r}\right)$ is the fundamental mode of the left sub-cavity of length r , and \bar{u}_k being the k -th mode of the right sub-cavity, and the inner product is with respect to the Klein-Gordon inner product. As shown in Appendix B 4, the modes $f_n(x)$ are orthogonal in the limit $R \gg r$, to $O(a^2)$, where $a = \frac{r}{L}$. In the limit of large g , the energy distributions now decouple and the left and right regions of the barrier r can be independently quantised, such that the energy distribution becomes

$$\hat{H}_R = \omega_1 \hat{a}_1^\dagger \hat{a}_1 + \sum_n \Omega_n \tilde{b}_n^\dagger \tilde{b}_n + \bar{\omega}_k \hat{a}_k^\dagger \hat{a}_k + g \hat{\phi}_\Delta(r) \hat{\phi}_\Delta(r). \quad (\text{B14})$$

This follows from breaking up the fundamental mode into two left and right sub-cavity modes, u_1, \bar{u}_k and proceeding with quantisation. Importantly this re-derives the standard membrane in the middle Hamiltonian [66] from a full quantum field theory picture (further seen by Taylor expanding $g(t) = \frac{i\omega r(t)}{1+r(t)}$ about reflectivities close to -1 , in which the interaction term picks up squeezing and beamsplitter terms with co-efficients proportional to $\omega_1(1+r(t))$). This branch-wise quantisation procedure then produces the following final Hamiltonian deriving the Hamiltonian given in the main text:

$$\hat{H} = \hat{H}_T \otimes |T\rangle_c \langle T|_c + \hat{H}_R \otimes |R\rangle_c \langle R|_c. \quad (\text{B15})$$

If we now expand the frequency-restricted field operator $\hat{\phi}_\Delta(r)$, in terms of global-cavity modes, and using for large g , that the mode functions scale as $\frac{k}{g}$. Now, taking $g(t)$ as above, where $r_{\text{eff}}(t)$ is the effective reflectivity and expanding for reflectivities close to zero. In the small g limit, the energy distribution becomes:

$$\hat{H}_R = \Omega_N \hat{b}_N^\dagger \hat{b}_N + \sum_n \Omega_{n \neq N} \hat{b}_n^\dagger \hat{b}_n + \Omega_N r_{\text{eff}}(t) \hat{\phi}_\Delta(r) \hat{\phi}_\Delta(r), \quad (\text{B16})$$

where $\Omega_N = \frac{\pi N}{L}$ is the global cavity mode N , and now expanding $\hat{\phi}_\Delta$ in terms of global cavity mode f_N . In particular the continuity condition in Eq. (B8), implies that the distinct energy distributions patch together, and can be diagonalised as $\Omega_N \hat{b}_N^\dagger \hat{b}_N$.

3. Non-adiabatic corrections

Here, as a further consistency check, we examine how for slow but finite switching rates, we obtain non-adiabatic corrections to the adiabatic theorem which still yields measurable photon content. We derive the same result using simple perturbation theory in a scalar field model, as well as a full QED analysis in which photonic field basis is time-dependent.

a. Scalar field model

Starting from the ground state of the global cavity, this typically implies that local sub-cavities will not show any particle content. In this Appendix, we show that this switching time still leads to non-adiabatic corrections that generate particle content

in the local sub-cavities. Specifically, we examine non-adiabatic corrections to the adiabatic theorem: that states that for slowly varying Hamiltonians the eigenstates track the Hamiltonian at each instant of time. Now considering a time-dependent reflection co-efficient, the interaction term in Eq. (B16) becomes time-dependent:

$$H_R(t) = \omega_1 \hat{a}_1^\dagger \hat{a}_1 + \bar{\omega}_k \hat{a}_k^\dagger \hat{a}_k + \sum_n \Omega_n \tilde{b}_n^\dagger \tilde{b}_n + \hat{H}_{\text{int}}(t), \quad (\text{B17})$$

Here, non-adiabatic corrections to the adiabatic theorem yield the amplitude to find the field excited to a higher energy state (to transition to instantaneous Hamiltonian eigenstate):

$$c_{1,k}^{(1)}(T) = - \int_0^T dt \frac{\langle m(t) | \dot{H}(t) | n(t) \rangle}{E_n(t) - E_m(t)} e^{i\phi_{nm}(t)}, \quad (\text{B18})$$

where T is the time-scale of the slow-switching, and $c_{1,k}^{(1)}$ is the amplitude for pairs of particles to be created across the sub-cavities by the two-mode squeezing interactions, in essence to transition to the $n = 1$ Fock state, due to squeezing. Here, $\phi_{nm}(t) = \theta_n(t) - \theta_m(t)$ and $\theta_n(t) \equiv -\frac{1}{\hbar} \int_0^t E_n(t') dt'$. For $\Gamma T \ll 1$, with the exponential rise of the reflectivity according to the linewidth, this produces $c_{1,k}^{(1)}(T) = r_{\max}(\frac{\Gamma_e}{\omega_1})$ being the leading corrections for the sub-cavity mode to transition due to non-adiabatic contributions. The power law suppression with the slow-switching switching time corroborates the predictions of the toy model for the scaling of the suppression of particle creation effects (in the sense of a power law suppression), and reduces to the previously studied single-mode-case in the relevant regime. This expression for the amplitude to transition due to a time-dependent boundary condition can also be re-written as the integral of the time-dependent frequency re-normalised from the time-dependent barrier (solved from the quantisation condition in Eq. (B9)), i.e.

$$c_{1,k}^{(1)}(T) = - \int_0^T dt \left(\frac{\dot{\omega}(t)}{\omega(t)} e^{i\phi_{nm}(t)} \right), \quad (\text{B19})$$

which we solve in the next section explicitly.

b. Quantum Electrodynamics

In order to re-derive the same particle creation through full QED using the state, we use as in section B 1 the dynamics of the electric field in the reflective branch of the superposition as

$$\partial_x^2 \hat{E} - \partial_t^2 \hat{E} = \frac{1}{\varepsilon_0} \partial_t^2 \hat{P}, \quad \hat{P}(t) = \alpha(t) \hat{E}^+(t) + \hat{S}_{\text{in}}, \quad (\text{B20})$$

with, $\alpha(t) = \frac{2i(\mu^k)^2}{\Gamma_e} (1 - e^{-\Gamma_e t/2})$, now taking the homogenous solution for the previously derived wave equation conditioned on the control atom's reflectivity (in which the input noise operator is an inhomogenous source term)

$$\partial_x^2 f(x, t) + k_0^2 f(x, t) = \frac{r(t) k_0}{2} f(x, t) \delta(x - r_x), \quad (\text{B21})$$

now taking $\hat{E}(x, t) = \sum_n \hat{q}_n(t) u_n(x, t)$, with $\partial_t^2 \hat{E} = \sum_n \ddot{\hat{q}}_n u_n + \dot{\hat{q}}_n \dot{u}_n + \hat{q}_n \ddot{u}_n$. Now with

$$\begin{aligned} M_{mn}(t) &\equiv \int dx u_m(x, t) \dot{u}_n(x, t) \\ K_{mn}(t) &= \int dx u_m(x, t) \ddot{u}_n(x, t), \end{aligned} \quad (\text{B22})$$

we obtain the Law-like equation,

$$\ddot{\hat{q}}_m + \omega_m^2(t) \hat{q}_m = - \sum_n M_{mn}(t) \dot{\hat{q}}_n - \sum_n K_{mn}(t) \hat{q}_n. \quad (\text{B23})$$

Now, the mode-mixing terms for $n \neq m$ are suppressed by the free-spectral-range compared to the effect of the $n = m$ terms. this corresponds to the equation. The modes here correspond to the modes of the instant-in-time modes in Eq.(B21). More

generally, if we define the instantaneous creation and annihilation operators,

$$\begin{aligned}\hat{a}_n(t) &\equiv \sqrt{\frac{\omega_n(t)}{2}}\hat{q}_n(t) + \frac{i}{\sqrt{2\omega_n(t)}}\hat{p}_n(t) \\ \hat{a}_n^\dagger(t) &\equiv \sqrt{\frac{\omega_n(t)}{2}}\hat{q}_n(t) - \frac{i}{\sqrt{2\omega_n(t)}}\hat{p}_n(t),\end{aligned}\tag{B24}$$

with, we obtain, the equation of motion of a harmonic oscillator with a time-dependent frequency,

$$\dot{\hat{a}}_n = -i\omega_n(t)\hat{a}_n + \frac{\dot{\omega}_n(t)}{2\omega_n(t)}\hat{a}_n^\dagger + \sqrt{\kappa_{\text{eff}}}\hat{\eta}(t),\tag{B25}$$

where we now have an effective input noise term with effective decay rate,

$$\kappa_{\text{eff}} = g_q^2 \frac{\Gamma_e}{\Gamma_e^2/4 + \Delta_e^2},\tag{B26}$$

on the photonic mode due to the coupling to the atomic polarisation operator, with correlator $\langle \hat{\eta}_{\text{in}}(t)\hat{\eta}_{\text{in}}^\dagger(t') \rangle \approx \delta(t - t')$.

Solving the particle production purely from the connection piece we have the analytical solution $\langle \hat{n} \rangle \approx \left(\frac{\Gamma_e}{N\omega_n}\right)^2$, consistent with the scaling computed from the scalar field model, with an additional factor corresponding to the global cavity mode number N . This is computed firstly by solving the Heisenberg Langevin equation with solution for the squeezing:

$$\hat{a}(t) = \hat{a}(t_0)e^{-i \int \omega(t)dt} + \beta(t)\hat{a}(t_0)^\dagger + \text{noise terms},\tag{B27}$$

where $\beta(t) = \frac{\dot{\omega}_n(t)}{2\omega_n(t)}e^{-i \int \omega(t)dt}$, and we solve for the time-dependent frequency by taking the total derivative of the quantisation condition in Eq. (B11), and expanding about reflectivities close to unity. More generally, integrating Eq. (B25), and restoring the implicit projector on the control atom's quantum state, and adding it to the global cavity energy distribution condition on the transmissive branch of the control that re-derives the effective dynamics corresponding to the Hamiltonian given in the main text (valid in the weak coupling limit for the Rabi drive on the control atom).

4. Alternative Reflective Hamiltonian Derivation

In this section, we construct an alternative derivation for the Hamiltonian for a cavity containing a reflective membrane that reflects only a single frequency by considering the allowed mode of the cavity field, which is relevant for the discussion at the end of Appendix B 2. In our quantum-controlled model, the Hamiltonian we construct here will correspond to the Hamiltonian of the photonic cavity when the atomic array is in its reflective state. We first consider the decomposition of the modes of a photonic cavity into its sub-regions, as described in Ref. [25]. The global cavity modes (\hat{b}_n) are related to the modes of the left and right sub-cavities (\hat{a}_l for the left sub-cavity and \hat{a}_l for the right sub-cavity) through the following Bogoliubov transformation, which gives the same Bogoliubov co-efficients as the inverse transformation in Eq. (3):

$$\hat{b}_n = \sum_l \alpha_{ln}\hat{a}_l - \beta_{ln}\hat{a}_l^\dagger + \bar{\alpha}_{ln}\hat{a}_l - \bar{\beta}_{ln}\hat{a}_l^\dagger,\tag{B28}$$

To isolate the contribution of a specific set of modes that are reflected by the array, we subtract the terms corresponding to those modes from the global mode expression. Specifically, by subtracting the contributions of the \hat{a}_1 mode (from the left sub-cavity) and the set of modes \hat{a}_k , with frequencies within the reflectivity bandwidth, $\bar{\omega}_k \in \Delta$ (from the right sub-cavity), we define a modified global mode \tilde{b}_n as:

$$\begin{aligned}\tilde{b}_n &= \hat{b}_n - \alpha_{1n}\hat{a}_1 + \beta_{1n}\hat{a}_1^\dagger + \sum_k -\bar{\alpha}_{kn}\hat{a}_k + \bar{\beta}_{kn}\hat{a}_k^\dagger \\ &= \sum_{l \geq 2} \alpha_{ln}\hat{a}_l - \beta_{ln}\hat{a}_l^\dagger + \sum_{l \neq k} \bar{\alpha}_{ln}\hat{a}_l - \bar{\beta}_{ln}\hat{a}_l^\dagger.\end{aligned}\tag{B29}$$

This explicitly subtracts the contributions of the \hat{a}_1 and \hat{a}_k modes, thereby modifying the global mode \hat{b}_n to exclude their contributions. If we now expand the global Hamiltonian in terms of each of the sub-cavity modes, and isolate out the contributions

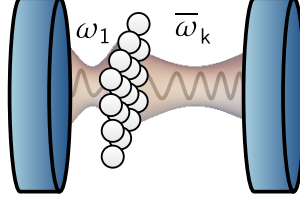


FIG. 5: An atom array in a photonic cavity that is highly reflective within some frequency band-width Δ , can trap standing waves of frequency $\omega_1 \in \Delta$ of the left sub-cavity, and $\bar{\omega}_k \in \Delta$ of the right sub-cavity. The Hamiltonian for an atom array that is highly reflective in this frequency band-width can be constructed as the sum of free Hamiltonian terms of the left and right sub-cavities, including vacuum terms.

from the single frequency sub-cavity modes \hat{a}_1 and $\hat{\tilde{a}}_k$ (this represents that when the mirror is off-centre, in general higher order modes $k \geq 1$ can be the frequency which is filtered by the mirror), we obtain

$$\begin{aligned}
 \hat{H}_T \rightarrow & \sum_n \left[\Omega_n \tilde{b}_n^\dagger \tilde{b}_n + \Omega_n \alpha_{1n} (\tilde{b}_n \hat{a}_1^\dagger + \hat{a}_1 \tilde{b}_n^\dagger) - \Omega_n \beta_{1n} (\hat{a}_1 \tilde{b}_n + \tilde{b}_n^\dagger \hat{a}_1^\dagger) + \Omega_n \left((\alpha_{1n}^2 + \beta_{1n}^2) \hat{a}_1^\dagger \hat{a}_1 \right) \right. \\
 & - \Omega_n \alpha_{1n} \beta_{1n} (\hat{a}_1^\dagger \hat{a}_1^\dagger + \hat{a}_1 \hat{a}_1) + \Omega_n \beta_{1n}^2 \left. \right] - \sum_k \left[\Omega_n \bar{\beta}_{kn} \left(\hat{\tilde{a}}_k \tilde{b}_n + \tilde{b}_n^\dagger \hat{\tilde{a}}_k^\dagger \right) - \Omega_n \bar{\alpha}_{kn} (\tilde{b}_n^\dagger \hat{\tilde{a}}_k + \hat{\tilde{a}}_k^\dagger \tilde{b}_n) \right. \\
 & + \Omega_n (\alpha_{1n} \bar{\alpha}_{kn} + \bar{\beta}_{kn} \beta_{1n}) (\hat{a}_1^\dagger \hat{\tilde{a}}_k + \hat{a}_1 \hat{\tilde{a}}_k^\dagger) - \Omega_n (\alpha_{1n} \bar{\beta}_{kn} + \bar{\alpha}_{kn} \beta_{1n}) (\hat{a}_1^\dagger \hat{\tilde{a}}_k^\dagger + \hat{a}_1 \hat{\tilde{a}}_k) \\
 & \left. + \Omega_n \left((\bar{\alpha}_{kn}^2 + \bar{\beta}_{kn}^2) \hat{\tilde{a}}_k^\dagger \hat{\tilde{a}}_k \right) - \Omega_n \bar{\alpha}_{kn} \bar{\beta}_{kn} \left(\hat{\tilde{a}}_k^\dagger \hat{\tilde{a}}_k^\dagger + \hat{\tilde{a}}_k \hat{\tilde{a}}_k \right) + \Omega_n \bar{\beta}_{kn}^2 \right]. \tag{B30}
 \end{aligned}$$

The presence of the single frequency mirror removes the interactions between the \hat{a}_1 mode and all right sub-cavity modes, as well as all $\hat{\tilde{a}}_k$ modes and all left sub-cavity modes. This follows how for the perfectly reflecting mirror considered in Sec. II, the effect of the mirror is to remove interactions and squeezing terms across the sub-cavity modes that are present in the global cavity Hamiltonian. Applying the same principle, but restricted to the set of frequencies reflected by the array (which was derived rigorously in Appendix B 2), we obtain,

$$\begin{aligned}
 \hat{H}_R &= \omega_1 \hat{a}_1^\dagger \hat{a}_1 + \sum_n \left[\Omega_n \tilde{b}_n^\dagger \tilde{b}_n + \Omega_n \beta_{1n}^2 \right] + \sum_k \left[\bar{\omega}_k \hat{\tilde{a}}_k^\dagger \hat{\tilde{a}}_k \right] + \sum_{k,n} \left[\Omega_n \bar{\beta}_{kn}^2 \right], \\
 &\simeq \omega_1 \hat{a}_1^\dagger \hat{a}_1 + \sum_n \Omega_n \tilde{b}_n^\dagger \tilde{b}_n + \sum_k \bar{\omega}_k \hat{\tilde{a}}_k^\dagger \hat{\tilde{a}}_k, \tag{B31}
 \end{aligned}$$

where the sum over k extends to all right sub-cavity modes that the single frequency mirror reflects (all modes that fall within the linewidth of the atomic array's reflectivity), and in the second line we have taken the limit $L \gg r$, where r is the size of the sub-cavity, and neglected all other terms as they are sub-leading in this regime. Importantly, in this regime, the dominant frequency shift between the transmissive and reflective states comes from difference in particle content, rather than constant offsets $\Omega_n \beta_{1n}^2$, $\Omega_n \bar{\beta}_{kn}^2$. The Hamiltonian of Eq. (B31) represents standing waves at the frequency ω_1 in the left sub-cavity, with standing waves of frequencies $\bar{\omega}_k$ in the right sub-cavity as displayed in Fig. 5. We now construct the Hamiltonian of the global cavity with the sub-cavities removed as

$$\hat{H}_\perp = \sum_n \Omega_n \tilde{b}_n^\dagger \tilde{b}_n, \tag{B32}$$

which is completely orthogonal to the individual single frequency sub-cavities as

$$[\hat{H}_\perp, \omega_1 \hat{a}_1^\dagger \hat{a}_1] = [\hat{H}_\perp, \bar{\omega}_k \hat{\tilde{a}}_k^\dagger \hat{\tilde{a}}_k] = 0. \tag{B33}$$

We therefore, use the following Hamiltonian for the single frequency reflective mirror in the $L \gg r$ regime,

$$\hat{H}_R = \omega_1 \hat{a}_1^\dagger \hat{a}_1 + \sum_n \Omega_n \tilde{b}_n^\dagger \tilde{b}_n + \sum_k \bar{\omega}_k \hat{\tilde{a}}_k^\dagger \hat{\tilde{a}}_k, \tag{B34}$$

noting that the commutator

$$\begin{aligned}
[\tilde{b}_i, \tilde{b}_j^\dagger] &= \delta_{ij} + \alpha_{1i}\alpha_{1j}^* - \beta_{1i}\beta_{1j}^* + \sum_k \bar{\alpha}_{ki}\bar{\alpha}_{kj}^* - \bar{\beta}_{ki}\bar{\beta}_{kj}^*, \\
&= \delta_{ij} + \frac{\sqrt{ij}(-1)^{i+j} \sin(i\pi a) \sin(j\pi a)}{\pi^2(a_j-1)(a_i-1)} - \frac{\sqrt{ij}(-1)^{i+j} \sin(i\pi a) \sin(j\pi a)}{\pi^2(a_j+1)(a_i+1)} \\
&\quad + \frac{k \sin(i\pi a) \sin(j\pi a)}{\sqrt{ij}\pi^2(\bar{a}'j-k)(\bar{a}'i-k)} - \frac{k \sin(i\pi a) \sin(j\pi a)}{\sqrt{ij}\pi^2(\bar{a}'j+k)(\bar{a}'i+k)}
\end{aligned} \tag{B35}$$

in the regime $L \gg r$, the commutator approaches $[\tilde{b}_i, \tilde{b}_j^\dagger] = \delta_{ij} + O(a^2)$, and we obtain a division of the sub-cavities in terms of purely orthogonal modes in this limit. With this form of the reflective Hamiltonian, the full quantum-controlled Hamiltonian in the main text follows from linearity. Alternatively, we can also use Eq. (B34), as an order of magnitude estimate for the $L \sim r$ regime, as the interaction terms between the modified global cavity modes \tilde{b}_n and the sub-cavity modes are sub-leading even in this regime compared to the free-energy terms, with the largest interaction terms being $O(0.5\Omega_n)$. Specifically we convert to the rotating frame of the free-energy terms and drop these terms as counter-rotating terms. Therefore, we use this Hamiltonian as the core model for all positions of the array through-out the cavity, however, the accuracy approaches unity for the $L \gg r$ regime.

Appendix C: Perturbative Dynamics

1. Analytical Estimate for the ideal frequency shift

In this section, we derive the analytical estimate for the frequency shift in the control due to particle-creation from the vacuum. The full Hamiltonian, in the rotating frame of the control atom is

$$\hat{H} = \hat{H}_{\text{cav}} + \hat{H}_{\text{switch}}, \tag{C1}$$

where,

$$\begin{aligned}
\hat{H}_{\text{cav}} &= \hat{H}_T \otimes |T\rangle\langle T| + \hat{H}_R \otimes |R\rangle\langle R| \\
\hat{H}_{\text{switch}} &= g \left(|T\rangle\langle R| e^{i(\omega_D - \nu)t} + \text{h.c.} \right),
\end{aligned} \tag{C2}$$

and we recall that $\hat{H}_T = \sum_n \Omega_n \hat{b}_n^\dagger \hat{b}_n$ and $\hat{H}_R = \omega_1 \hat{a}_1^\dagger \hat{a}_1 + \sum_n \Omega_n \tilde{b}_n^\dagger \tilde{b}_n + \sum_k \bar{\omega}_k \hat{a}_k^\dagger \hat{a}_k$. Now, we can express $\hat{a}_1^\dagger \hat{a}_1$ in terms of the global modes as

$$\omega_1 \hat{a}_1^\dagger \hat{a}_1 = \sum_n \left(\omega_n \hat{b}_n^\dagger \hat{b}_n - g_n \hat{b}_n^\dagger \hat{b}_n^\dagger - g_n^* \hat{b}_n \hat{b}_n + \omega_1 |\beta_{1,n}|^2 \right) + \sum_{n \neq m} \left(f_{n,m} \hat{b}_n^\dagger \hat{b}_m - g_{n,m} \hat{b}_n^\dagger \hat{b}_m^\dagger - g_{m,n}^* \hat{b}_n \hat{b}_m + f_{n,m}^* \hat{b}_n \hat{b}_m^\dagger \right). \tag{C3}$$

where,

$$\begin{aligned}
\omega_n &= \omega_1 \left(|\alpha_{1,n}|^2 + |\beta_{1,n}|^2 \right), \\
f_{n,m} &= \omega_1 \alpha_{1,n} \alpha_{1,m}^*, \\
g_n &= \omega_1 \alpha_{1,n} \beta_{1,n}^*, \\
g_{n,m} &= \omega_1 \alpha_{1,n} \beta_{1,m}^*.
\end{aligned} \tag{C4}$$

We now convert into the rotating frame of $\hat{H}_T \otimes |R\rangle\langle R|$, and drop all of the counter-rotating terms, and then when converting back out of the rotating frame, we are left with the $\sum_n \omega_n \hat{b}_n^\dagger \hat{b}_n$ term. This produces the Hamiltonian:

$$\hat{H}_{\text{cav}} = \hat{H}_T \otimes |T\rangle\langle T| + \left(\sum_n \left(\omega_n \hat{b}_n^\dagger \hat{b}_n + \Omega_n \hat{b}_n^\dagger \hat{b}_n + \Omega_n \tilde{b}_n^\dagger \tilde{b}_n + \omega_1 |\beta_{1,n}|^2 \right) + \sum_k \bar{\omega}_k \hat{a}_k^\dagger \hat{a}_k \right) \otimes |R\rangle\langle R|, \tag{C5}$$

and, as derived previously, after conversion to the interaction picture,

$$P_R = g^2 \int_0^t dt' dt'' \langle 0_T | e^{i\hat{H}_R(t'-t'')} | 0_T \rangle e^{i(\omega_D - \nu)(t'-t'')} \quad (C6)$$

gives the probability for the control atom to transition from the transmissive to the reflective state. The analytical estimate for the frequency shift

$$\delta_R = \sum_n \omega_1 |\beta_{1,n}|^2, \quad (C7)$$

provides a good approximation of the precise numerical solution. We have omitted the contribution from the $\sum_n \tilde{b}_n^\dagger \tilde{b}_n$ term in the Hamiltonian, as we numerically evaluate its contribution to be sub-leading, while the dominant contribution to the frequency shift evaluates to be $\sum_n |\beta_{1,n}|^2 \simeq 0.075$, in the regime $L \gg r$. This is the frequency shift which we use in the main text, and serves as an order of magnitude approximation in the regime for which $L \sim r$, as the additional interaction terms are sub-leading in this regime, which we confirmed through a numerical diagonalisation including all terms.

2. Perturbative Dynamics of a Quantum-Controlled Photonic Cavity

Here we present a perturbative analytical solution of the dynamics of a quantum-controlled photonic cavity. To derive this, we consider the full Hamiltonian, including the free Hamiltonian of the control:

$$\hat{H} = \frac{\hbar\nu}{2} (|R\rangle\langle R| - |T\rangle\langle T|) + \hat{H}_T \otimes |T\rangle\langle T| + \hat{H}_R \otimes |R\rangle\langle R| + g(|T\rangle\langle R| e^{+i\omega_D t} + |R\rangle\langle T| e^{-i\omega_D t}), \quad (C8)$$

which includes a drive applied on the control atom of strength g and frequency ω_D . Now transforming to the rotating frame of the control, produces:

$$\hat{H} \rightarrow e^{i\hat{H}_{\text{free}}t/\hbar} \hat{H} e^{-i\hat{H}_{\text{free}}t/\hbar} = \hat{H}_T \otimes |T\rangle\langle T| + \hat{H}_R \otimes |R\rangle\langle R| + g(|T\rangle\langle R| e^{i(\omega_D - \nu)t} + |R\rangle\langle T| e^{i(\nu - \omega_D)t}), \quad (C9)$$

where $\hat{H}_{\text{free}} = (\hbar\nu/2)(|R\rangle\langle R| - |T\rangle\langle T|)$ is the free Hamiltonian of the control. We now break up the following contributions to the Hamiltonian:

$$\begin{aligned} \hat{H}_0 &= \hat{H}_T \otimes |T\rangle\langle T| + \hat{H}_R \otimes |R\rangle\langle R| \\ \hat{H}_g &= g(|T\rangle\langle R| e^{i(\omega_D - \nu)t} + |R\rangle\langle T| e^{-i(\omega_D - \nu)t}). \end{aligned} \quad (C10)$$

We treat \hat{H}_g as a perturbation, and work in the interaction picture:

$$\hat{H}_g(t) = e^{i\hat{H}_0 t} \hat{H}_g e^{-i\hat{H}_0 t}. \quad (C11)$$

we have $|\psi(t)\rangle_I = e^{i\hat{H}_0 t} |\psi(t)\rangle_S = U_I(t) |\psi_I(0)\rangle$, where

$$U_I(t) = \mathcal{T} \left\{ e^{-i \int_0^t dt' \hat{H}_g(t')} \right\} = \hat{\mathbb{I}} - i \int_0^t dt' \hat{H}_g(t') - \frac{1}{2} \int_0^t dt' \int_0^{t'} dt'' \hat{H}_g(t') \hat{H}_g(t'') + \dots, \quad (C12)$$

where \mathcal{T} denotes time-ordering. Including terms up to second order in g , gives explicitly

$$\begin{aligned}
\hat{U}_I^{(2)} &= \hat{\mathbb{I}} - ig \int_0^t dt' (e^{i\hat{H}_T t'} |T\rangle \langle R| e^{-i\hat{H}_R t'} e^{i(\omega_D - \nu)t'} + \text{h.c.}) \\
&\quad - \frac{g^2}{2} \int_0^t dt' \int_0^{t'} dt'' (e^{i\hat{H}_T t'} |T\rangle \langle R| e^{-i\hat{H}_R t'} e^{i(\omega_D - \nu)t'} + \text{h.c.}) (e^{i\hat{H}_T t''} |T\rangle \langle R| e^{-i\hat{H}_R t''} e^{i(\omega_D - \nu)t''} + \text{h.c.}) + O(g^2) \\
&= \hat{\mathbb{I}} - ig \int_0^t dt' (e^{i\hat{H}_T t'} |T\rangle \langle R| e^{-i\hat{H}_R t'} e^{i(\omega_D - \nu)t'} + \text{h.c.}) \\
&\quad - \frac{g^2}{2} \int_0^t dt' \int_0^{t''} dt'' (e^{i\hat{H}_T t'} |T\rangle \langle R| e^{-i\hat{H}_R t'} e^{i\hat{H}_T t''} |T\rangle \langle R| e^{-i\hat{H}_R t''} e^{i(\omega_D - \nu)(t' + t'')} \\
&\quad + e^{i\hat{H}_T t'} |T\rangle \langle R| e^{-i\hat{H}_R t'} e^{i\hat{H}_R t''} |R\rangle \langle T| e^{-i\hat{H}_T t''} e^{i(\omega_D - \nu)(t' - t'')} \\
&\quad + e^{i\hat{H}_R t'} |R\rangle \langle T| e^{-i\hat{H}_T t'} e^{i\hat{H}_T t''} |T\rangle \langle R| e^{-i\hat{H}_R t''} e^{-i(\omega_D - \nu)(t' - t'')} \\
&\quad + e^{i\hat{H}_R t'} |R\rangle \langle T| e^{-i\hat{H}_T t'} e^{i\hat{H}_R t''} |R\rangle \langle T| e^{i\hat{H}_T t''} e^{-i(\omega_D - \nu)(t' + t'')}) + O(g^3).
\end{aligned} \tag{C13}$$

In the main text, this unitary is restricted to $O(g)$ terms relevant for the leading order computations of the transition rate of the control atom. If the control is initially in the transmissive state, the probability for it to flip to the reflective state after unitary evolution up to $O(g)$ is

$$P_R = g^2 \int_0^t dt' dt'' \langle 0_T | e^{i\hat{H}_R(t' - t'')} | 0_T \rangle e^{i(\omega_D - \nu)(t' - t'')}, \tag{C14}$$

which is used in the main text. The higher order terms correspond to Lamb-shift-type energy corrections.

3. Imperfect Reflectivity

Here, we outline a toy model for switching on a mirror of imperfect reflectivity. Our model for a mirror with imperfect reflectivity is adapted from Ref. [49], which considers particle content due to the presence of a time-dependent boundary condition at the origin of Minkowski spacetime, as well as that of a cavity with boundaries at $x = \pm a/2$. A similar problem was considered in Ref. [67], for a mirror following conformal diamond time with tunable reflectivity.

As elsewhere in this manuscript, we consider a real massless scalar field $\hat{\phi} \equiv \hat{\phi}(t, x)$. Introducing a mirror at $x = 0$ modifies the scalar Klein-Gordon equation to read,

$$\partial_t^2 \hat{\phi} - \Delta_{\theta(t)} \hat{\phi} = 0 \tag{C15}$$

where $\{-\Delta_\theta | \theta \in [0, \pi/2]\}$ is the one-parameter family of self-adjoint extensions of $-\partial_x^2$ on $L^2(\mathbb{R} \setminus \{0\})$. The limiting cases $\theta(t) = 0, \pi/2$ correspond to a perfectly reflective and transmissive boundary respectively, with intermediate values interpolating between the two. One can write Eq. (C15) as,

$$\left[\partial_t^2 - \partial_x^2 + \frac{2 \cot(\theta(t))}{L} \delta(x) \right] \hat{\phi} = 0 \tag{C16}$$

where L has dimensions of length, which we henceforth set to unity. The presence of the mirror thus acts as a potential term proportional to $\delta(x)$ with a time-dependent coefficient, tending to zero as $\theta \rightarrow (\pi/2)_-$ and to $+\infty$ as $\theta \rightarrow 0_+$. Following Ref. [49], we take $\theta(t)$ to be

$$\theta(t) = \tan^{-1} \left(\frac{1 + e^{-\lambda t}}{\lambda} \right) \tag{C17}$$

as discussed in the main text. Since $0 < \theta(t) < \pi/2$, the mirror exists for all t , but it is never Dirichlet. It is perfectly transmissive in the asymptotic past, indicated by the limit $\theta(t) \rightarrow \pi/2$ as $t \rightarrow -\infty$, and its ‘‘formation’’ (i.e. its ability to reflect cavity modes)

begins exponentially slowly. The end state of the mirror in the asymptotic future is not perfectly reflecting (Dirichlet), since $\theta(t) \rightarrow \cot^{-1}(\lambda)$ as $t \rightarrow \infty$; however, it can be made arbitrarily close to Dirichlet by allowing λ to be large. To obtain the mode functions with frequency k , we make the ansatz,

$$U_k(u, v) = \frac{1}{\sqrt{8\pi k}} \left[e^{-ikv} + E_k(u) \right] \quad (\text{C18})$$

where $v = t + x$, $u = t - x$ are lightcone coordinates and $E_k(u)$ is to be found. Note that the spatially odd solutions to the field equation Eq. (C15) do not feel the presence of the wall; only the spatially even solutions do. By spatial evenness, it suffices to consider these solutions in the half-space $x > 0$, where those in the space $x < 0$ follow by the replacement $(t, x) \rightarrow (t, -x)$. If we restrict ourselves, for simplicity, to the right-moving modes, then it can be shown that the constraints imposed by Eq. (C16) imply solutions of the form,

$$E_k(u) = R_{k/\lambda}(\lambda u) \quad (\text{C19})$$

where

$$R_K(y) = \begin{cases} e^{-iKy} & y \leq 0 \\ e^{-iKy} - \frac{2}{B(y)} \int_0^y B'(y') e^{-iKy'} dy' & 0 < y < 1 \\ -e^{-iKy} & y \geq 1 \end{cases} \quad (\text{C20})$$

and $B(y)$ is a solution to $B'(y)/B(y) = \cot(h(y))$ with the initial condition $B(0) = 1$, with $h(y) = \tan^{-1}(1 + e^{-y})$. For this choice of $h(y)$, the right-moving modes during the switching are given by [49]

$$\bar{U}_k(u) = \frac{1}{\sqrt{8\pi k}} \frac{e^{-iku}}{1 + e^{\lambda u}} \left(1 - \frac{\lambda + ik}{\lambda - ik} e^{\lambda u} \right). \quad (\text{C21})$$

Henceforth, we work with the cavity modes explicitly, which can be obtained from Eq. (C21) by replacing the prefactor $(8\pi k)^{-1/2}$ with $(4\pi m)^{-1/2}$ where $m \in \mathbb{Z}$ and restricting $k = \pi m/a$. Meanwhile, the standing wave solutions of the global cavity are simply $U_m(u) = (4\pi m)^{-1/2} e^{-i\pi mu/a}$. We can expand the subcavity mode operators \hat{a}_m in a basis of the global mode operators $(\hat{b}_n, \hat{b}_n^\dagger)$ via the Bogoliubov transformation,

$$\hat{a}_m = \sum_{n=1}^{+\infty} \left(\alpha_{nm} \hat{b}_n + \beta_{nm} \hat{b}_n^\dagger \right) \quad (\text{C22})$$

where the Bogoliubov coefficients α_{nm}, β_{nm} are defined in the usual way via the Klein-Gordon inner product. In the vacuum of the unperturbed modes, the expectation value of the particle number of the new modes is,

$$\langle 0_B | \hat{a}_m^\dagger \hat{a}_m | 0_B \rangle = \sum_{n=1}^{+\infty} |\beta_{nm}|^2 \quad (\text{C23})$$

It now remains to compute the Bogoliubov coefficients $\beta_{k\omega}$, which are given by

$$\beta_{nm} = \langle U_m^\star(u), \bar{U}_n(u) \rangle = i \int_0^{a/2} du \left(U_m(u) \partial_u \bar{U}_n - \bar{U}_n \partial_u U_m \right) \quad (\text{C24})$$

Upon integration, one obtains,

$$\begin{aligned} \beta_{nm} = & \frac{1}{4\pi} \sqrt{\frac{n}{m}} \left(\frac{ie^{-ia\vartheta\lambda}}{\vartheta\lambda} {}_2F_1 \left(1 - i\vartheta, 1 - i\vartheta, -e^{a\lambda/2} \right) + \frac{1}{2\lambda} \left(\psi^{(0)}(-i\theta/2) - \psi^{(0)}(-i\theta/2 + 1/2) \right) \right) \\ & - \frac{1}{4\pi} \sqrt{\frac{n}{m}} \frac{\lambda + i\pi m/a}{\lambda - i\pi m/a} \left(\frac{i}{2\vartheta\lambda} \left(2\text{Re} \left[e^{ia\vartheta\lambda} {}_2F_1 \left(1, -i\theta, -i\theta + 1, -e^{a\lambda/2} \right) \right] - \pi\vartheta \text{csch}(\pi\theta) - 1 \right) \right. \\ & \left. + \frac{1}{2\theta\lambda} \left(2\text{Re} \left[ie^{-ia\vartheta\lambda} {}_2F_1 \left(1, i\theta, i\theta + 1, -e^{-a\lambda/2} \right) \right] - \vartheta \text{Re} \left[\psi^{(0)}(-i\theta/2) - \psi^{(0)}(-i\theta/2 + 1/2) \right] \right) \right) \end{aligned} \quad (\text{C25})$$

where ${}_2F_1(\alpha, \beta, \gamma, z)$ is the hypergeometric function, $\psi^{(0)}(z)$ is the PolyGamma function [68], and we defined $\vartheta = (m + n)\pi/(a\lambda)$. Substituting Eq. (C25) into Eq. (C23) gives the average particle number $\langle \hat{N} \rangle$ in Fig. 3(b) of the main text.

Taylor expanding the effective reflectivity for short times, we obtain for small λ , that its behaviour at short times scales as $O(-t\lambda^2)$. This indicates that a single order of magnitude reduction in λ , corresponds to a two order of magnitude reduction in the reflectivity rise time-scale. In this way, if we associate $\lambda = 20$ with a fast 10-100 femtosecond time-scale, $\lambda \sim 2 \times 10^{-3}$, corresponds to a micro-second scale of the switching time. This slower reflectivity switch produces particle content on the order of 5×10^{-8} , corresponding to a six order of magnitude reduction in the frequency shift. This indicates that a measurable tail of the frequency shift will survive that is larger than the linewidth of the control atom. Furthermore the toy model agrees with the behaviour of the reflectivity switch in the reflective branch of the superposition solved from the full model of microscopic interactions in Appendix A, after associating λ^2 with the eigenvalues of the matrix of ODEs of the dynamics for the atomic amplitudes (in the sense of a power law suppression).

4. Non-Perturbative Transition Calculations and Cavity Intensity

If the control atom is driven off-resonance, there should be a substantially reduced probability for the control atom to flip to its reflective state. As expected for weak couplings, such that $g \ll \nu \sim \omega_1$, the standard off-resonant suppression expected in the quantum optical Rabi model is observed, scaling as g^2 :

$$c_R = \frac{g^2}{\Omega^2} \sin^2(\Omega t/2), \quad (\text{C26})$$

where $\Omega = [(\delta + \delta_R)^2 + g^2]^{1/2}$. This implies for the cavity extraction protocol, that when the cavity is driven on-resonance with the sub-cavity frequency ω_1 , that the average intensity observed in the cavity, will be suppressed by the non-zero probability for the atom array to be in the reflective state $|c_R|^2$. The intensity of light in the cavity close to the sub-cavity frequency is

$$I = \frac{I_{\max} |c_R|^2}{1 + (2\mathcal{F}/\pi)^2 \sin^2(\pi\nu_P/\omega_1)}, \quad (\text{C27})$$

where $I_{\max} = \frac{I_0}{(1-r)^2}$, \mathcal{F} is the finesse of the cavity, r is the optical attenuation factor due to any imperfect reflectivity of the array and ν_P is the frequency of the pump. In this way, a substantial average power will only be observed in the cavity at the sub-cavity frequency, if the control atom was driven at the re-normalised frequency due to the presence of photons from entangled sub-regions of the vacuum of the global cavity.

Appendix D: Comparison to the Dynamical Casimir Effect and the Lamb Shift

1. Parametric Forms of the Dynamical Casimir Effect

In this section, we compare the particle creation phenomena considered in this work with parametric forms of the DCE, in which the effect can be described with a Bogoliubov expansion truncated to a single mode expansion. In the case for which the larger sub-cavity length is approximately the global cavity length, such that $\frac{r-L}{L} \ll 1$, the Bogoliubov relation between the modes can be truncated at lowest order in the expansion,

$$\hat{a}_j \simeq \alpha_{jj} \hat{b}_j - \beta_{jj} \hat{b}_j^\dagger, \quad (\text{D1})$$

In this case, the Hamiltonian of the sub-cavity transforms as:

$$\hat{H} = \sum_j \omega_j \hat{a}_j^\dagger \hat{a}_j \rightarrow \sum_j \omega_j (|\alpha_{jj}|^2 + |\beta_{jj}|^2) \hat{b}_j^\dagger \hat{b}_j - \omega_j \alpha_{jj} \beta_{jj} (\hat{b}_j^\dagger \hat{b}_j^\dagger + \hat{b}_j \hat{b}_j) + \omega_j |\beta_{jj}|^2, \quad (\text{D2})$$

now to quadratic order in the Bogoliubov expansion we use that $|\alpha_{jj}|^2 - |\beta_{jj}|^2 \simeq 1$, in this perturbative regime, and we see that the Hamiltonian simplifies to the free-energy term of the global cavity, plus a squeezing term:

$$\hat{H} \rightarrow \sum_j \omega_j \hat{a}_j^\dagger \hat{a}_j \rightarrow \sum_j \omega_j \hat{b}_j^\dagger \hat{b}_j - \omega_j \alpha_{jj} \beta_{jj} (\hat{b}_j^\dagger \hat{b}_j^\dagger + \hat{b}_j \hat{b}_j) + \omega_j |\beta_{jj}|^2. \quad (\text{D3})$$

In this perturbative regime, we can see the time-dependent boundary condition produces parametric generation of pairs of photons in each cavity mode. If the cavity is driven with a drive frequency ω_D , with the cavity initially in the ground state the probability to produce pairs of photons in the cavity is $P_j(|n=2\rangle) = \omega_j^2 \alpha_{jj}^2 \beta_{jj}^2 t^2 \text{sinc}^2((\omega_D - 2\omega_j)t)$. This corresponds

to the resonant production of pairs of photons in the cavity, comparable to the parametric generation of cavity photons due to the motion of a mirror in blue-detuned regime of optomechanical set-ups [60]. In this sense, parametric forms of the DCE, can be interpreted as the parametric generation of photon pairs from a resonant drive as in optomechanical set-ups, not particle content due to entanglement between spatially distinct sub-systems, or particle creation from a fundamentally altered photonic mode structure from a time-dependent boundary condition. Indeed, all DCE experiments to date can be interpreted as the parametric coupling of unperturbed and time-independent cavity modes. In this way, our proposal allows probing fundamental physics neither tested nor discussed in the related albeit distinct context of the existing DCE experiments. Furthermore, we note that defining the detuning $\Delta = \omega_D - 2\omega_j$, we find for fixed interaction times, a quadratic suppression of the particle creation probability with the detuning, indicating the scaling of the suppression of particle creation for the adiabatic regime (slow switching).

More concretely, we model the Bogoliubov transformation with time-dependent Bogoliubov coefficients, modelling a time-dependent change in cavity length or equivalently refractive index or susceptibility of a medium:

$$\hat{H} = \sum_j \omega_j \hat{a}_j^\dagger \hat{a}_j, \quad (\text{D4})$$

with time-dependent Bogoliubov transformation:

$$\hat{a}_j(t) \rightarrow \alpha_{jj}(t) \hat{b}_j - \beta_{jj}(t) \hat{b}_j^\dagger, \quad (\text{D5})$$

If we use this transformation in the Hamiltonian, the Hamiltonian transforms as

$$\tilde{H}(t) = S(t) \hat{H}_0(t) S^\dagger(t) - i S(t) \dot{S}^\dagger(t), \quad (\text{D6})$$

such that $S(t)$ is a Bogoliubov transformation that implements the squeezing operation, $\hat{a}_j = S(t) \hat{b}_j S^\dagger(t)$, $\hat{a}_j^\dagger = S^\dagger(t) \hat{b}_j^\dagger S(t)$:

$$\hat{S}(t) \dot{S}^\dagger(t) = \frac{\dot{\zeta}^*(t)}{2} \hat{b}^{\dagger 2} - \frac{\dot{\zeta}(t)}{2} \hat{b}^2, \quad (\text{D7})$$

where $\alpha = \cosh(|\zeta(t)|)$, $\beta = -\sinh(|\zeta(t)|)$. Identifying the Bogoliubov coefficients with squeezing parameters, we can write the transformed Hamiltonian in Eq. (D6) as:

$$\tilde{H}(t) = \omega(|\alpha_{jj}|^2 + |\beta_{jj}|^2) \left(\hat{b}_j^\dagger \hat{b}_j + \frac{1}{2} \right) + \hbar C(t) \hat{b}_j^{\dagger 2} + \hbar C^*(t) \hat{b}_j^2, \quad (\text{D8})$$

where the combination of the additional term from Eq. (D7), as well as the transformation from Eq. (D5) give squeezing coefficient

$$C(t) = -\omega_j \alpha_{jj}(t) \beta_{jj}(t) - i \dot{\zeta}^*(t). \quad (\text{D9})$$

In the slow-switching regime, the first term here $\omega_j \alpha_{jj} \beta_{jj}$ corresponds to corrections to the free Hamiltonian and therefore the new vacuum state due to the time-dependent boundary conditions (the mismatch with the initial vacuum state which previously resulted in particle content), while the second term will result in non-adiabatic corrections, and is clearly a factor of $\frac{\gamma}{\omega_j}$ (where γ is the slow rate of change of the time-dependent coefficients) smaller in terms of order of magnitude once the finite switching rate is taken into account. In this way, the quantum state under the drive Hamiltonian evolves as (according to the adiabatic theorem, to lowest order in the unitary evolution),

$$|\psi(t)\rangle \simeq |0_{a_j}\rangle |T\rangle + (gt) |0_{\bar{b}_j}\rangle |R\rangle \quad (\text{D10})$$

where $\hat{a}_j |0_{a_j}\rangle = 0$, and $|0_{\bar{b}_j}\rangle$ is the vacuum state with respect to the free Hamiltonian and adiabatically shifting squeezing terms, up to the non-adiabatic corrections defined above. Importantly, such non-adiabatic corrections quantified as above produce the signature frequency shift by shifting out of this vacuum state by the factor $\frac{\gamma}{\omega_j}$.

2. Comparison to the Lamb Shift

Computing the energy shift of the excited state of the control atom due to emission or absorption of a virtual photon into the vacuum (as in the Lamb shift) produces a quantitatively distinct frequency shift. Most notably, the leading contribution to the Lamb shift occurs at second order in perturbation theory, whereas the shift we consider here is non-vanishing at leading order.

Furthermore, the Lamb shift applies to energy corrections for processes where the input and output states are identical, whereas our analysis involves transitions between different Fock states of the photonic field. Higher order terms in the Dyson expansion also involve Lamb-shift-type energy corrections, that depend on the different energy distributions of the two sub-cavity regions. This can be seen if we take the second order term in the unitary evolution operator, which involve frequency shifts due to transitions between the same energy states of the control:

$$\begin{aligned}
\hat{U}_T^{\text{Lamb}} = & -\frac{g^2}{2} \int_0^t dt' \int_0^{t''} dt'' \left(e^{i\hat{H}_T t'} |T\rangle \langle R| e^{-i\hat{H}_R t'} e^{i\hat{H}_T t''} |T\rangle \langle R| e^{-i\hat{H}_R t''} e^{i(\omega_D - \nu)(t' + t'')} \right. \\
& + e^{i\hat{H}_T t'} |T\rangle \langle R| e^{-i\hat{H}_R t'} e^{i\hat{H}_R t''} |R\rangle \langle T| e^{-i\hat{H}_T t''} e^{i(\omega_D - \nu)(t' - t'')} \\
& + e^{i\hat{H}_R t'} |R\rangle \langle T| e^{-i\hat{H}_T t'} e^{i\hat{H}_T t''} |T\rangle \langle R| e^{-i\hat{H}_R t''} e^{-i(\omega_D - \nu)(t' - t'')} \\
& \left. + e^{i\hat{H}_R t'} |R\rangle \langle T| e^{-i\hat{H}_T t'} e^{i\hat{H}_R t''} |R\rangle \langle T| e^{i\hat{H}_T t''} e^{-i(\omega_D - \nu)(t' + t'')} \right) + O(g^3),
\end{aligned} \tag{D11}$$

and we can see that this produces an energy shift that depends on the energy of the reflective and transmissive branches respectively, for transitions from the $|T\rangle$ state to the $|T\rangle$ state, as well as the $|R\rangle$ state to the $|R\rangle$ state. We leave a detailed analysis of the dynamics of such Lamb-shift type corrections to future work.

3. Evidence for Vacuum Entanglement and Outlook

While the vacuum particle content discussed here, either in the fast or slow switching regime is fundamentally a signature of genuine vacuum particle creation, in the fast-switching regime it can also be considered to be a signature of the entanglement structure of the vacuum. If the global cavity is initially prepared in a pure state—which can be set up and verified experimentally before driving the control—then the Schmidt criterion applies: Sub-systems whose matrices are not rank-1 are necessarily entangled. Measuring the rank in this way would require tomography of the quantum state of the sub-regions of the global cavity, which is an interesting problem beyond the scope of this work. However, we highlight that such sub-region particle content remains a testable prediction of the standard entanglement structure of the electromagnetic vacuum, and more intricate schemes can be developed in future protocols to verify that the sub-region photon content is necessarily from the entanglement structure of the vacuum rather than noise. In this way, the experimental implementation of our proposal in the fast-switching regime would not only mark the first observation of the local particle content of the vacuum, a seminal yet hitherto untested prediction of QFT, but also serve as the first experimental signature of the entanglement structure of the vacuum.

Our proposal further explores a novel regime of light–matter interaction by implementing dynamics of superpositions of macroscopically distinct photonic QED vacua, motivating the experimental realisation and exploration of fundamental phenomena in QFT. This includes the simulation of quantum effects arising due to dynamics of superpositions of spacetimes, whereby the configuration of a source mass and its effect on fields plays an analogous role to the state of the array [69, 70]. This platform also enables the observation of Rabi oscillations affected by the entangled vacuum’s local particle content, offering a novel quantum-enhanced probe of the frame-dependent particle content central to QFT in curved spacetime [11], and it is an open question as to whether it could enable the observation of quantum reference frame [71] dependent particle content. In particular, it allows controlled access to the photon content perceived by observers in a superposition of trajectories [72, 73]. In general, the here-proposed platform enables a novel type of vacuum particle creation, in which the process is coherently superposed with the absence of particle creation. Our proposal extends the quantum-optical interaction of light and matter and state-dependent boundary conditions [74–77] (involving entanglement of a quantum control with an optical degree of freedom in a cavity QED setting) into the unexplored domain in which the quantum-control determines macroscopically distinct photonic vacuum structures, paving the way towards a new class of near-term experiments that bridge quantum optics, relativistic quantum information, quantum field theory and quantum sensing.

[1] H. Reeh and S. Schlieder, Bemerkungen zur unitäräquivalenz von lorentzinvarianten feldern, *Nuovo cimento* **22**, 1051 (1961).
[2] S. J. Summers and R. Werner, The vacuum violates bell’s inequalities, *Physics letters. A* **110**, 257 (1985).
[3] E. Witten, Aps medal for exceptional achievement in research: Invited article on entanglement properties of quantum field theory, *Rev. Mod. Phys.* **90**, 045003 (2018).
[4] H. Casini and M. Huerta, Entanglement entropy in free quantum field theory, *Journal of Physics A: Mathematical and Theoretical* **42**, 504007 (2009).

[5] M. R. Vázquez, M. del Rey, H. Westman, and J. León, Local quanta, unitary inequivalence, and vacuum entanglement, *Annals of Physics* **351**, 112 (2014).

[6] J. Keaveney, A. Sargsyan, U. Krohn, I. G. Hughes, D. Sarkisyan, and C. S. Adams, Cooperative Lamb shift in an atomic vapor layer of nanometer thickness, *Physical review letters* **108**, 173601 (2012).

[7] R. B. Hutson, W. R. Milner, L. Yan, J. Ye, and C. Sanner, Observation of millihertz-level cooperative Lamb shifts in an optical atomic clock, *Science (American Association for the Advancement of Science)* **383**, 384 (2024).

[8] G. T. Moore, Quantum theory of the electromagnetic field in a variable-length one-dimensional cavity, *Journal of mathematical physics* **11**, 2679 (1970).

[9] S. A. Fulling and P. C. W. Davies, Radiation from a moving mirror in two dimensional space-time: Conformal anomaly, *Proceedings of the Royal Society of London. Series A, Mathematical and physical sciences* **348**, 393 (1976).

[10] P. C. W. Davies and S. A. Fulling, Radiation from moving mirrors and from black holes, *Proceedings of the Royal Society of London. Series A, Mathematical and physical sciences* **356**, 237 (1977).

[11] N. D. Birrell and P. C. W. Davies, *Quantum Fields in Curved Space*, Cambridge Monographs on Mathematical Physics (Cambridge University Press, 1982).

[12] S. W. Hawking, Black hole explosions?, *Nature (London)* **248**, 30 (1974).

[13] S. R. Wadia and S. W. Hawking, Particle creation by black holes, *Resonance* **26**, 133 (2021).

[14] W. G. Unruh, Notes on black-hole evaporation, *Phys. Rev. D* **14**, 870 (1976).

[15] L. C. B. Crispino, A. Higuchi, and G. E. A. Matsas, The unruh effect and its applications, *Rev. Mod. Phys.* **80**, 787 (2008).

[16] H.-T. Zheng, X.-F. Zhou, G.-C. Guo, and Z.-W. Zhou, Enhancing analog unruh effect via superradiance in a cylindrical cavity, *Physical review research* **7**, 013027 (2025).

[17] A. Deswal, N. Arya, K. Lochan, and S. K. Goyal, *Time-resolved and superradiantly amplified unruh signal* (2025), [arXiv:2501.16219 \[quant-ph\]](https://arxiv.org/abs/2501.16219).

[18] D. Su, C. T. M. Ho, R. B. Mann, and T. C. Ralph, Quantum circuit model for non-inertial objects: a uniformly accelerated mirror, *New Journal of Physics* **19**, 063017 (2017).

[19] V. Dodonov, Fifty years of the dynamical casimir effect, *Physics* **2**, 67 (2020).

[20] T.-D. Chung and H. Verlinde, Dynamical moving mirrors and black holes, *Nuclear Physics B* **418**, 305 (1994).

[21] C. Holzhey, F. Larsen, and F. Wilczek, Geometric and renormalized entropy in conformal field theory, *Nuclear physics b* **424**, 443 (1994).

[22] M. R. R. Good, E. V. Linder, and F. Wilczek, Moving mirror model for quasithermal radiation fields, *Phys. Rev. D* **101**, 025012 (2020).

[23] I. Akal, Y. Kusuki, N. Shiba, T. Takayanagi, and Z. Wei, Holographic moving mirrors, *Classical and Quantum Gravity* **38**, 224001 (2021).

[24] C. M. Wilson, G. Johansson, A. Pourkabirian, M. Simeon, J. R. Johansson, T. Duty, F. Nori, and P. Delsing, Observation of the dynamical Casimir effect in a superconducting circuit, *Nature (London)* **479**, 376 (2011).

[25] E. G. Brown, M. del Rey, H. Westman, J. León, and A. Dragan, What does it mean for half of an empty cavity to be full?, *Physical Review D* **91** (2015).

[26] M. Johanning, A. F. Varón, and C. Wunderlich, Quantum simulations with cold trapped ions, *Journal of physics. B, Atomic, molecular, and optical physics* **42**, 154009 (2009).

[27] M. Endres, H. Bernien, A. Keesling, H. Levine, E. R. Anschuetz, A. Krajenbrink, C. Senko, V. Vuletic, M. Greiner, and M. D. Lukin, Atom-by-atom assembly of defect-free one-dimensional cold atom arrays, *Science* **354**, 1024 (2016).

[28] A. Browaeys and T. Lahaye, Many-body physics with individually controlled rydberg atoms, *Nature physics* **16**, 132 (2020).

[29] N. Arya and M. Zych, Selective amplification of a gravitational wave signal using an atomic array (2024), [arXiv:2408.12436 \[quant-ph\]](https://arxiv.org/abs/2408.12436).

[30] M. A. Norcia, H. Kim, W. B. Cairncross, M. Stone, A. Ryou, M. Jaffe, M. O. Brown, K. Barnes, P. Battaglino, T. C. Bohdanowicz, A. Brown, K. Cassella, C.-A. Chen, R. Coxe, D. Crow, J. Epstein, C. Griger, E. Halperin, F. Hummel, A. M. W. Jones, J. M. Kindem, J. King, K. Kotru, J. Lauigan, M. Li, M. Lu, E. Megidish, J. Marjanovic, M. McDonald, T. Mittiga, J. A. Muniz, S. Narayanaswami, C. Nishiguchi, T. Paule, K. A. Pawlak, L. S. Peng, K. L. Pudenz, D. Rodríguez Pérez, A. Smull, D. Stack, M. Urbanek, R. J. M. van de Verdonk, Z. Vendeiro, L. Wadleigh, T. Wilkason, T.-Y. Wu, X. Xie, E. Zalys-Geller, X. Zhang, and B. J. Bloom, Iterative assembly of ^{171}Yb atom arrays with cavity-enhanced optical lattices, *PRX Quantum* **5**, 030316 (2024).

[31] R. Tao, M. Ammenwerth, F. Gyger, I. Bloch, and J. Zeiher, High-fidelity detection of large-scale atom arrays in an optical lattice, *Phys. Rev. Lett.* **133**, 013401 (2024).

[32] D. Porras and J. I. Cirac, Collective generation of quantum states of light by entangled atoms, *Physical Review A—Atomic, Molecular, and Optical Physics* **78**, 053816 (2008).

[33] R. Bekenstein, I. Pikovski, H. Pichler, E. Shahmoon, S. F. Yelin, and M. D. Lukin, Quantum metasurfaces with atom arrays, *Nature physics* **16**, 676 (2020).

[34] F. Shah, T. L. Patti, O. Rubies-Bigorda, and S. F. Yelin, Quantum computing with subwavelength atomic arrays, *Phys. Rev. A* **109**, 012613 (2024).

[35] N. Antman Ron, M. Carmi, and R. Bekenstein, Atom-atom entanglement generation via collective states of atomic rings, *Physical Review Research* **6**, L042051 (2024).

[36] D. Castells-Graells, J. I. Cirac, and D. S. Wild, Cavity quantum electrodynamics with atom arrays in free space, *Phys. Rev. A* **111**, 053712 (2025).

[37] S. R. Hastings, M. J. A. de Dood, H. Kim, W. Marshall, H. S. Eisenberg, and D. Bouwmeester, Ultrafast optical response of a high-reflectivity gaas alas bragg mirror, *Applied Physics Letters* **86**, 031109 (2005).

[38] K. Srakaew, P. Weckesser, S. Hollerith, D. Wei, D. Adler, I. Bloch, and J. Zeiher, A subwavelength atomic array switched by a single rydberg atom, *Nature physics* **19**, 714 (2023).

[39] H. Wang, M. P. Blencowe, C. M. Wilson, and A. J. Rimberg, Mechanically generating entangled photons from the vacuum: A microwave circuit-acoustic resonator analog of the oscillatory unruh effect, *Phys. Rev. A* **99**, 053833 (2019).

[40] X. Ma and W. Rhodes, Multimode squeeze operators and squeezed states, *Physical review. A, Atomic, molecular, and optical physics* **41**,

4625 (1990).

[41] J. Wang, D.-Y. Huang, X.-L. Zhou, Z.-M. Shen, S.-J. He, Q.-Y. Huang, Y.-J. Liu, C.-F. Li, and G.-C. Guo, Ultrafast high-fidelity state readout of single neutral atom, *Physical review letters* **134**, 240802 (2025).

[42] D. B. Branden, T. Juhasz, T. Mahlokozera, C. Vesa, R. O. Wilson, M. Zheng, A. Kortyna, and D. A. Tate, Radiative lifetime measurements of rubidium rydberg states, *Journal of Physics B: Atomic, Molecular and Optical Physics* **43**, 015002 (2009).

[43] A. Frisk Kockum, A. Miranowicz, S. De Liberato, S. Savasta, and F. Nori, Ultrastrong coupling between light and matter, *Nature reviews physics* **1**, 19 (2019).

[44] A. Kumar, A. Suleymanzade, M. Stone, L. Taneja, A. Anferov, D. I. Schuster, and J. Simon, Quantum-enabled millimetre wave to optical transduction using neutral atoms, *Nature (London)* **615**, 614 (2023).

[45] E. Shahmoon, D. S. Wild, M. D. Lukin, and S. F. Yelin, Cooperative resonances in light scattering from two-dimensional atomic arrays, *Physical review letters* **118**, 113601 (2017).

[46] H. Levine, A. Keesling, G. Semeghini, A. Omran, T. T. Wang, S. Ebadi, H. Bernien, M. Greiner, V. Vuletić, H. Pichler, and M. D. Lukin, Parallel implementation of high-fidelity multiqubit gates with neutral atoms, *Phys. Rev. Lett.* **123**, 170503 (2019).

[47] E. Shahmoon, M. D. Lukin, and S. F. Yelin, Quantum optomechanics of a two-dimensional atomic array, *Phys. Rev. A* **101**, 063833 (2020).

[48] M. Eltohfa and F. Robicheaux, Effects of finite trapping on the decay, recoil, and decoherence of dark states of quantum emitter arrays (2025), [arXiv:2502.09851 \[physics.atom-ph\]](https://arxiv.org/abs/2502.09851).

[49] E. G. Brown and J. Louko, Smooth and sharp creation of a dirichlet wall in 1+1 quantum field theory: how singular is the sharp creation limit?, *The journal of high energy physics* **2015**, 1 (2015).

[50] V. Dodonov and A. Klimov, Long-time asymptotics of a quantized electromagnetic field in a resonator with oscillating boundary, *Physics Letters A* **167**, 309 (1992).

[51] V. V. Dodonov and A. B. Klimov, Generation and detection of photons in a cavity with a resonantly oscillating boundary, *Phys. Rev. A* **53**, 2664 (1996).

[52] A. Lambrecht, M.-T. Jaekel, and S. Reynaud, Motion induced radiation from a vibrating cavity, *Phys. Rev. Lett.* **77**, 615 (1996).

[53] H. Wang and M. Blencowe, Coherently amplifying photon production from vacuum with a dense cloud of accelerating photodetectors, *Communications physics* **4**, 1 (2021).

[54] B. P. Dolan, A. Hunter-McCabe, and J. Twamley, Shaking photons from the vacuum: acceleration radiation from vibrating atoms, *New Journal of Physics* **22**, 033026 (2020).

[55] V. Macrì, A. Ridolfo, O. Di Stefano, A. F. Kockum, F. Nori, and S. Savasta, Nonperturbative dynamical Casimir effect in optomechanical systems: Vacuum Casimir-Rabi splittings, *Physical review. X* **8**, 011031 (2018).

[56] E. Russo, A. Mercurio, F. Mauceri, R. Lo Franco, F. Nori, S. Savasta, and V. Macrì, Optomechanical two-photon hopping, *Phys. Rev. Res.* **5**, 013221 (2023).

[57] A. Ferreri, V. Macrì, F. K. Wilhelm, F. Nori, and D. E. Bruschi, Quantum field heat engine powered by phonon-photon interactions, *Phys. Rev. Res.* **5**, 043274 (2023).

[58] A. Ferreri, D. E. Bruschi, F. K. Wilhelm, F. Nori, and V. Macrì, Phonon-photon conversion as mechanism for cooling and coherence transfer, *Phys. Rev. Res.* **6**, 023320 (2024).

[59] A. Mercurio, E. Russo, F. Mauceri, S. Savasta, F. Nori, V. Macrì, and R. L. Franco, Bilateral photon emission from a vibrating mirror and multiphoton entanglement generation, *SciPost Phys.* **18**, 067 (2025).

[60] M. Aspelmeyer, T. J. Kippenberg, and F. Marquardt, Cavity optomechanics, *Rev. Mod. Phys.* **86**, 1391 (2014).

[61] E. Shahmoon, D. S. Wild, M. D. Lukin, and S. F. Yelin, Cooperative resonances in light scattering from two-dimensional atomic arrays, *Phys. Rev. Lett.* **118**, 113601 (2017).

[62] F. Li, An analytical model for transient evolution of eit-at spectrum with rydberg atoms, *Optics letters* **50**, 1369 (2025).

[63] M. T. Manzoni, M. Moreno-Cardoner, A. Asenjo-Garcia, J. V. Porto, A. V. Gorshkov, and D. E. Chang, Optimization of photon storage fidelity in ordered atomic arrays, *New journal of physics* **20**, 83048 (2018).

[64] C. Gardiner, Input and output in damped quantum systems iii: formulation of damped systems driven by fermion fields, *Optics Communications* **243**, 57 (2004), ultra Cold Atoms and Degenerate Quantum Gases.

[65] J. Haro and E. Elizalde, Hamiltonian approach to the dynamical casimir effect, *Phys. Rev. Lett.* **97**, 130401 (2006).

[66] A. M. Jayich, J. C. Sankey, B. M. Zwickl, C. Yang, J. D. Thompson, S. M. Girvin, A. A. Clerk, F. Marquardt, and J. G. E. Harris, Dispersive optomechanics: a membrane inside a cavity, *New journal of physics* **10**, 095008 (2008).

[67] J. Foo, S. Onoe, M. Zych, and T. C. Ralph, Generating multi-partite entanglement from the quantum vacuum with a finite-lifetime mirror, *New Journal of Physics* **22**, 083075 (2020).

[68] I. S. Gradshteyn and I. M. Ryzhik, *Table of integrals, series, and products* (Academic press, 2014).

[69] J. Foo, C. S. Arabaci, M. Zych, and R. B. Mann, Quantum signatures of black hole mass superpositions, *Phys. Rev. Lett.* **129**, 181301 (2022).

[70] A.-C. de la Hamette, V. Kabel, E. Castro-Ruiz, and C. Brukner, Quantum reference frames for an indefinite metric, *Communications physics* **6**, 231 (2023).

[71] F. Giacomini, E. Castro-Ruiz, and C. Brukner, Quantum mechanics and the covariance of physical laws in quantum reference frames, *Nature communications* **10**, 494 (2019).

[72] J. Foo, S. Onoe, and M. Zych, Unruh-dewitt detectors in quantum superpositions of trajectories, *Phys. Rev. D* **102**, 085013 (2020).

[73] L. C. Barbado, E. Castro-Ruiz, L. Apadula, and i. C. Brukner, Unruh effect for detectors in superposition of accelerations, *Phys. Rev. D* **102**, 045002 (2020).

[74] K. M. Gheri and H. Ritsch, Single-atom quantum gate for light, *Phys. Rev. A* **56**, 3187 (1997).

[75] B. Wang and L.-M. Duan, Engineering superpositions of coherent states in coherent optical pulses through cavity-assisted interaction, *Phys. Rev. A* **72**, 022320 (2005).

- [76] W. J. M. Kort-Kamp, A. K. Azad, and D. A. R. Dalvit, Space-time quantum metasurfaces, *Phys. Rev. Lett.* **127**, 043603 (2021).
- [77] K. Sinha, J. Parra-Contreras, A. Das, and P. Solano, Spontaneous emission in the presence of quantum mirrors, *New Journal of Physics* **27**, 054101 (2025).

ACKNOWLEDGEMENTS

We thank the participants of the Swedish workshop on analogue gravity, as well as Navdeep Arya, Simon Hollerith, Robert Mann, Eduardo Martin-Martinez, Rick Perche, Igor Pikovski, and Johannes Zeiher for discussions. This material is based upon work supported by the Knut and Alice Wallenberg foundation through a Wallenberg Academy Fellowship No. 2021.0119, and the General Sir John Monash Foundation. J.F. acknowledges funding provided by the Natural Sciences and Engineering Research Council of Canada through a Banting Postdoctoral Fellowship. SQ is funded in part by the Wallenberg Initiative on Networks and Quantum Information (WINQ) and in part by the Marie Skłodowska–Curie Action IF programme *Nonlinear optomechanics for verification, utility, and sensing* (NOVUS) – Grant-Number 101027183. Nordita is supported in part by NordForsk.